International Journal of Engineering Research & Technology (IJERT)
ISSN: 2278-0181
Vol. 15 Issue 11 , November - 2026

Numerical Modeling and Optimization of Lead-Free Perovskite Solar Cells via SCAPS-1D: Evaluating Back-Contact Work Functions and Transport Dynamics

Ali AlMahmoud, Kaesar Alyamani, Omar AlAli, Hussein AlHussein
Ph.D. in Physics, Department of Physics, Faculty of Science, University of Aleppo
Assistant Professor, Department of Physics, Faculty of Science, Al -furat University
Ph.D. in Physics, Department of Physics, Faculty of Science, University of Aleppo
Ph.D. in Physics, Department of Physics, Faculty of Science, University of Aleppo
Ph.D. in Physics, Department of Physics, Faculty of Science, University of Aleppo

Abstract - This text provides a precise and comprehensive review of back-contact engineering and numerical simulation methodologies for lead-free perovskite solar cells (LF-PSCs). It delves into the fundamental obstacles and complex physical and chemical challenges that hinder the commercialization and widespread adoption of lead-free absorber materials—specifically tin-based perovskites ($ASnX_3$) and lead-free double perovskites (such as $Cs_2AgBiBr_6$). A primary focus of the text is the significant limitations imposed by the back interface. Mismatches in energy levels, unfavorable work-function differences between the perovskite absorber and traditional noble-metal back contacts (e.g., gold), and the formation of a Schottky barrier severely impede charge extraction and lead to parasitic energy losses. To overcome these interface-related constraints, the text examines advanced processing strategies, including back-contact engineering tailored to specific material compositions, the integration of chemically stable, dopant-free inorganic hole-transport layers (HTLs)—such as NiO_x and CuSCN—and the adoption of carbon-based electrodes and graphene derivatives (e.g., rGO) as scalable alternatives to noble metals. Furthermore, the text highlights the vital role of numerical simulation—specifically using the "drift-diffusion" model via the SCAPS-1D software—as an essential predictive tool for modeling device physics, optimizing layer thicknesses, and analyzing the energy landscape prior to experimental fabrication. The text also underscores the critical need for advanced interface passivation techniques and the incorporation of molecular interlayers (such as specialized carboxylic compounds and antioxidant additives). These measures serve to mitigate non-radiative recombination, prevent the interdiffusion of halides and metals, and suppress the spontaneous oxidation of tin ions (Sn^{2+}) into Sn^{4+}—a process that leads to the degradation of cell performance. Ultimately, the review asserts that the back contact can no longer be treated merely as a passive electrical collector; rather, it must be viewed as a purposefully engineered functional interface—a vital component for achieving long-term operational stability and high power-conversion efficiencies in lead-free photovoltaic cell technologies.

Keywords:

Lead-Free Perovskite Solar Cells (LF-PSCs), Back-Contact Engineering, Numerical Simulation (SCAPS-1D), Interface Passivation, Carbon-based Electrodes, Work Function Matching, Tin-based Perovskites, Charge Carrier Extraction Dynamics

1. INTRODUCTION

The rapid development of solar energy over the past two decades has established photovoltaics as the fastest-growing and most cost-competitive source of new electricity generation worldwide, as documented in successive global status assessments and energy outlook reports [1,2]. Nevertheless, the market remains dominated by crystalline silicon, a technology now approaching its practical limits; reassessments of the limiting-efficiency framework indicate little remaining headroom for mass-produced single-junction silicon modules [4,5]. This has motivated decades of research into third-generation concepts that circumvent the

(This work is licensed under a Creative Commons Attribution 4.0 International License.)

International Journal of Engineering Research & Technology (IJERT)
ISSN: 2278-0181
Vol. 15 Issue 11 , November - 2026

single-junction limit while reducing cost [6]. Among emerging thin-film technologies, metal-halide perovskite solar cells (PSCs) have attracted exceptional attention: since the first sensitization reports [7] and the demonstration of efficient meso-superstructured devices [8], certified power-conversion efficiencies (PCEs) have risen from 3.8% to more than 26% [4,9], enabled by compositional and interfacial engineering such as atomically coherent interlayers [12], cesium triple-cation formulations [13], and two-dimensional Ruddlesden–Popper architectures [14], with extension to tandem, indoor, flexible, and semi-transparent applications [10,11].

The outstanding photovoltaic performance of PSCs originates from a rare combination of optoelectronic properties: high absorption coefficients, tunable bandgaps, low exciton binding energies, long carrier diffusion lengths, and remarkable defect tolerance [15,20,21,22]. The structural flexibility of the ABX_3 lattice additionally allows cation and anion compositions to be tuned over a wide range without destroying the perovskite phase.

Despite this progress, most high-efficiency devices still rely on lead-containing absorbers such as $MAPbI_3$, $FAPbI_3$, and related Cs–Pb halides [23,24]. The toxicity and water solubility of lead raise serious environmental concerns during manufacturing, operation, and disposal, triggering regulatory restrictions and a broad search for safer alternatives [25,26,27,28]. Replacing lead is non-trivial: the substituting element must simultaneously match the ionic radius, reproduce the lone-pair ns^2 defect physics, and offer a suitable band structure. Divalent tin (Sn^{2+}) is the closest homolog of Pb^{2+}, and lead-free absorbers based on $CsSnI_3$, $FASnI_3$, $MASnI_3$, $CsSnBr_3$, and mixed-halide $CsSn(I_{1-x}Br_x)_3$ have therefore received the most attention [28–35].

Electronic similarity between Sn^{2+} and Pb^{2+}, however, does not translate into equivalent chemical stability. Sn^{2+} is readily oxidized to Sn^{4+} under ambient conditions, generating tin vacancies (V_Sn) that act as shallow acceptors and produce strong p-type self-doping, degraded carrier lifetimes, and irreproducible performance [36–40]. Managing this intrinsic instability through compositional design and careful interface control remains the central challenge of tin-based photovoltaics.

The back contact is particularly important because it determines how efficiently photogenerated holes are extracted and how much voltage is lost parasitically at the rear interface [44–47]. In the conventional n–i–p architecture, the rear electrode must form an ohmic contact to the hole-transport layer (HTL) while blocking recombination and acting as a barrier against iodide and metal-ion migration. Poor energetic alignment between the HTL valence band and the electrode Fermi level produces a Schottky-type barrier at the rear interface, manifesting in S-shaped (kinked) J–V characteristics, depressed fill factors, and reduced open-circuit voltage [80,81]. Gold ($\Phi \approx 5.1$ eV) is the reference high-work-function electrode, but its cost and its propensity to diffuse into the stack motivate systematic evaluation of cheaper metals (Ag, Cu, Al, transition metals) whose work functions frequently fall below the threshold required for ohmic hole extraction [45,46,82–85,87].

Carbon-based contacts are promising alternatives to noble metals. Electrodes prepared as pastes, graphite, carbon black, carbon nanotubes, graphene, and reduced graphene oxide combine low cost, chemical inertness, hydrophobicity, and high work functions, and have enabled stable HTL-free architectures in both lead-based and tin-based perovskites [54,86–88]. Reduced graphene oxide offers an additional degree of freedom, since its effective work function can be tuned by the degree of reduction and surface functionalization, enabling deliberate work-function engineering rather than passive electrode selection [88,89, 116].

Numerical device simulation provides a complementary route to understanding — and ultimately designing — the rear interface. One-dimensional drift-diffusion solvers, most prominently SCAPS-1D, allow the back-contact work function, transport-layer thickness and doping, and interfacial defect densities to be swept systematically at negligible experimental cost, and have been widely used to rationalize contact-selection strategies for $CsSnI_3$, $FASnI_3$, $MASnI_3$, and related lead-free absorbers [30,37,40,45,52,63,64,66,69,74–76,78,81,88,90–92]. Benchmarking such models against experimentally calibrated reference cells — for example, the $CsSnI_3$ baseline with a gold contact [100] — allows numerical predictions to be translated into actionable design rules, such as the work-function threshold of approximately 5.0–5.1 eV above which S-shaped kinks disappear and the fill factor recovers.

(This work is licensed under a Creative Commons Attribution 4.0 International License.)

International Journal of Engineering Research & Technology (IJERT)
ISSN: 2278-0181
Vol. 15 Issue 11 , November - 2026

Despite the growing number of numerical and experimental studies, a systematic, cross-comparative treatment of back-contact engineering in lead-free perovskites remains scarce. Published results are scattered across a diverse family of absorbers, device architectures, and simulation assumptions, obscuring which conclusions are material-specific and which are general [33–35,46,48,52,66,74,84,86–89]. This review is motivated by the need for a unified picture of the rear interface as an integrated component of the lead-free device stack; the thematic analysis and citation framework presented here are grounded in the source manuscript , which supplies both the section structure and the numbered reference list reproduced below.The objectives of this review are fourfold. First, we elucidate the physical and chemical principles governing energetic alignment at the rear interface, including work-function matching, Fermi-level pinning, and Schottky-barrier formation [79,81]. Second, we evaluate the viability of low-cost alternatives to noble-metal electrodes, with emphasis on carbon-based and rGO-derived contacts [52,82,83]. Third, we analyze the degradation mechanisms operating specifically at the rear interface — metal diffusion, halide migration, and interfacial oxidation — and the passivation strategies developed to suppress them [84,85]. Fourth, we identify critical design rules and numerical insights derived from SCAPS-1D modeling and experimentally calibrated reference devices [30,91,92,100], culminating in practical guidelines for contact selection.

1.1. $Cs_2AgBiBr_6$ Double Perovskite

Although tin perovskites are characterized by narrow and favorable energy gaps, their susceptibility to oxidation remains a major limitation. Double perovskites offer an alternative approach to developing lead-free adsorbents. In these structures, the two Pb^{2+} sites are replaced by two different ions, typically one monovalent and one trivalent. $Cs_2AgBiBr_6$ is one of the most studied examples, where Ag^{++} and Bi3+ occupy the two sublattices of the B site. Compared to many tin perovskites, $Cs_2AgBiBr_6$ exhibits relatively good structural, thermal, and environmental stability [66–69]. It can also be deposited as a lead-free thin film [67, 68]. The main drawbacks of $Cs_2AgBiBr_6$ are its relatively large and predominantly indirect band gap, typically ranging from 1.9 to 2.2 eV, depending on the layer quality and measurement conditions [69, 70]. The indirect band gap reduces absorption near the absorption edge and may necessitate the use of thicker absorption layers. Furthermore, deep defects, poor layer morphology, short charge carrier diffusion distances, and interfacial recombination can limit device efficiency. These limitations make contact geometry critical for this composite [101- 110]. Efficient back contact for $Cs_2AgBiBr_6$ must efficiently extract holes while minimizing the valence band barrier and suppressing electron leakage to the back electrode. Both hole-transporting layers (HTLs) and hole-free structures, including those using carbon electrodes, have been investigated. Carbon is an attractive option due to its low cost, chemical stability, and compatibility with printing processes. However, the carbon/cesium interface may require: Passive surface treatment of $Cs_2AgBiBr_6$ or a selective intermediate layer to reduce contact resistance and facilitate non-radiative recombination [111-115, 74]. This example illustrates that chemical stability alone is insufficient; the contact must also provide suitable energy alignment and low-defect charge transfer.

1.2. Low-Dimensional and Vacuum-Structured Adsorbents

Antimony and bismuth compounds, including Cs_3Sb_2 and $Cs_3Bi_2I_9$, have been studied as lead-free light-absorbing materials [74]. These materials are typically described as perovskite-inspired, perovskite-like, or vacuum-structured, rather than perfect three-dimensional perovskites [75]. Depending on the phase and processing conditions, their structure may contain isolated [Sb_2I_9] and [Bi_2I_9] molecules, or weakly bonded ones. This low dimensionality strongly affects light absorption, charge transport, and defect behavior. The main advantage of $Cs_3Sb_2I_9$ and $Cs_3Bi_2I_9$ is their low toxicity and potential for improved chemical durability compared to lead- and tin-based absorbers [75, 76]. However, their low dimensionality may lead to increased charge concentration and reduced charge transport over long distances. These properties increase the importance of the conductive layers and electrical interconnects. In particular, a suitable back conductor should, as far as possible, compensate for the poor charge transport while avoiding additional barriers and recombination at the interface. Therefore, these materials should not be evaluated using the same conductor selection rules developed for narrow-bandgap three-dimensional tin perovskites.

1.3. Role of Charge-Transport Layers and Back Contacts

Although the absorber controls much of the optical response, the final photovoltaic performance is determined by the complete device architecture. The electron-transport layer (ETL), hole-transport layer (HTL), front electrode, and back contact must operate as an integrated system. An absorber with a suitable

(This work is licensed under a Creative Commons Attribution 4.0 International License.)

International Journal of Engineering Research & Technology (IJERT)
ISSN: 2278-0181
Vol. 15 Issue 11 , November - 2026

bandgap and high absorption coefficient may still produce poor device performance if an interface contains a large energetic barrier or a high density of recombination centers [45,77,78]. The back contact performs several related functions. It extracts photogenerated holes, transfers them to the external circuit, and completes the electrical path through the device. It also influences the built-in electric field and band bending near the rear interface. Depending on its structure and microstructure, it may also provide some protection against moisture, oxygen, and volatile species. In addition, the conductivity of the electrode and the quality of its interface with the adjacent layer directly affect the series resistance, Rs. A high Rs reduces the fill factor and limits the output current, particularly near the maximum-power point [79]. For effective hole extraction, the back electrode should exhibit favorable energy-level alignment with the absorber or HTL. In a simplified model, a high-work-function electrode is generally preferred because it can reduce the energetic barrier for hole collection [78,79]. However, work function alone cannot fully describe the behavior of a real interface. Interface dipoles, chemical reactions, Fermi-level pinning, surface states, interdiffusion, roughness, and local defects can all modify the effective alignment. Consequently, the measured electrical response may differ substantially from the prediction based only on the isolated work functions of the two materials.

Poor alignment can lead to the formation of a Schottky-type barrier at the rear interface. Such a barrier may cause hole accumulation, reduce extraction efficiency, and increase interfacial recombination. It may also produce current–voltage rollover or an S-shaped J_V curve. By contrast, a well-designed contact can approach ohmic behavior, facilitate hole transport, and reduce losses in voltage and fill factor [80,81]. This distinction is particularly important for p-type tin absorbers because their high background hole concentration and defect-sensitive interfaces can significantly modify the depletion region. Gold is frequently used as the back electrode in conventional PSCs. Its high conductivity, relatively high work function, and resistance to atmospheric oxidation often support efficient hole collection [45,46]. It is therefore commonly used as a reference contact in experimental studies and numerical simulations [82-84]. However, gold is expensive and is not attractive for cost-sensitive, large-area manufacturing. It may also diffuse through organic or defective transport layers under thermal and electrical stress. In addition, reactions between gold and halide species may contribute to long-term degradation. Silver is less expensive than gold and has excellent conductivity, but it can react with mobile halide ions and form silver halides [84,85]. Copper is inexpensive and conductive, although copper diffusion and oxidation may reduce device stability. Aluminum is abundant and low-cost, but its relatively low work function can create an unfavorable hole-extraction barrier in many device structures. Transition metals such as Ni, Mo, W, Cr, and Fe offer a broad range of work functions and chemical properties, but their suitability depends on the absorber composition, the use of an HTL, and the chemical stability of the rear interface [46,47,87].

Carbon-based contacts are promising alternatives to noble metals. Carbon paste, graphite, carbon black, carbon nanotubes, graphene-related materials, and reduced graphene oxide can offer low cost, chemical stability, abundance, and compatibility with printing or low-temperature processing [86,87]. Carbon electrodes may also reduce the risk of metal-ion migration. However, their electrical and interfacial properties depend strongly on composition, surface functionalization, porosity, processing temperature, and binder content. A rough or poorly wetted carbon layer may produce weak physical contact with the absorber and increase the series resistance [54,88]. Carbon should therefore be regarded as a broad class of materials rather than as a single electrode with fixed properties. Reduced graphene oxide and related rGO-based contacts provide additional opportunities because their work function and conductivity can be modified by controlling the degree of reduction, defect concentration, doping, and surface functional groups. These factors may improve energy alignment with different lead-free absorbers. At the same time, residual oxygen-containing groups can alter the electrical properties and may influence interfacial chemical stability. Thus, the performance of rGO contacts depends not only on their nominal composition but also on their reduction state, defect structure, morphology, and interaction with the neighboring layer [88,89].

1.4. Scope and Motivation of the Review

Despite the growing number of numerical and experimental studies on lead-free perovskite solar cells, a unified and systematic evaluation of back-contact requirements across different absorber families remains scarce. The substantial diversity among lead-free absorbers poses a fundamental challenge:

a back contact optimized for one material cannot be assumed to yield comparable performance in another [81,88]. These materials differ significantly in their intrinsic properties, including energy bandgap, electron affinity, valence-band position, dielectric constant, charge-carrier density, defect chemistry, and structural

(This work is licensed under a Creative Commons Attribution 4.0 International License.)

International Journal of Engineering Research & Technology (IJERT)
ISSN: 2278-0181
Vol. 15 Issue 11 , November - 2026

dimensionality [30,40,76]. For instance, narrow-bandgap tin iodides provide high photocurrents but suffer from rapid Sn2+ oxidation and severe p-type self-doping [37,40]. Incorporating bromide widens the bandgap and alters band-edge positions, shifting the energetic requirements for hole extraction [63,64]. Double perovskites such as $Cs_2AgBiBr_6$ Offer superior ambient stability but are hindered by a wide, indirect bandgap and low carrier mobility [66,69]. Meanwhile, low-dimensional and vacancy-ordered structures ($Cs_3Sb_2I_9$) and $Cs_3Bi_2I_9$) present distinct carrier localization dynamics that cannot be treated with conventional 3D transport assumptions [75,76]. Consequently, selecting an optimal back contact requires an integrated assessment of the absorber–contact interface rather than relying solely on the bulk electrical conductivity or isolated work function of the electrode [45,78]. Numerical simulation, particularly via SCAPS-1D, provides a robust and cost-effective approach to model these complex interfacial phenomena before carrying out extensive laboratory fabrication [90–92]. It enables detailed investigation into energy-band alignment, carrier generation and recombination, interface defect states, series resistance (Rs), operating temperature, and work-function sensitivity. When calibrated against reliable experimental data, numerical modeling allows researchers to decouple intrinsic absorber losses from interfacial extraction barriers and resistive parasitic effects [91]. Accordingly, this review provides a comprehensive comparative evaluation of back-contact engineering and numerical modeling across representative lead-free perovskite absorber families. CsSnI3 serves as the primary benchmark system, while $FASnI_3$,$MASnI_3$,$CsSnBr_3$, and mixed-halide $CsSn(I_{1-x}Br_x)_3$ represent organic–inorganic, all-inorganic, and compositional tunability in tin-based systems [33–35,48]. In addition,Cs2AgBiBr6, represents double perovskite architectures, and Cs3Sb2I9, Cs3Bi2I9 represent low-dimensional, perovskite-inspired systems [66,74]. Particular emphasis is placed on comparing conventional noble metals—primarily gold (Au) with low-cost alternative electrodes, including transition metals (Al, Cr ,Mo ,Cu ,Ag ,Fe,Ni ,W), carbon pastes, and reduced graphene oxide (rGO)-based contacts [46,84,86,87,89]. These electrodes, covering a broad work-function range (typically 4.41 to 5.22 eV), are analyzed across both HTL-based and HTL-free device configurations [52,88].

The primary objectives of this review are to:

- Elucidate the physical and chemical principles governing back-contact operation, including work-function matching, Schottky barrier formation, Fermi-level pinning, defect-assisted interfacial recombination, and chain resistance [79,81].
- Evaluate the viability of low-cost alternatives to noble metals, assessing whether carbon and transition metals can prevent major deficits in open-circuit voltage (Voc), short-circuit current density (Jsc), fill factor (FF), and power conversion efficiency (PCE) [52,82,83].
- Analyze degradation mechanisms at the rear interface, specifically metal-ion migration, halide reactions, and chemical stability under thermal and ambient stress [84,85].
- Identify critical design rules and numerical insights to guide future experimental validation and accelerate the development of efficient, stable, and cost-effective lead-free perovskite photovoltaics [30,91,92].

2. FUNDAMENTALS OF BACK-CONTACT AND INTERFACE PHYSICS IN PSCS

2.1. Surface Recombination, Contact Resistance, and Parasitic Losses:

Even when energy bands are compatible, the back surface can limit device performance through surface recombination, contact resistance, and parasitic losses [93-95]. These losses reduce hole extraction efficiency, lower the fill factor, and decrease the open-circuit voltage. In lead-free perovskite solar cells, these losses are critical because many absorber material compositions already suffer from high defect density, short charge carrier diffusion lengths, and chemical instability [93, 94]. Surface recombination occurs when photogenerated charge carriers reach defect-rich regions near the back contact and recombine before extraction. This process is typically described by Shockley-Red-Hall (SRH) statistics, where trap states act as recombination centers. High surface defect density increases the rate of local recombination and weakens charge carrier selectivity [93-96]. As a result, the back contact no longer acts as a passive collector but becomes an active loss site. This is often reflected in a low open-circuit voltage (V_{oc}), a poor fill factor (F_F), and sometimes a device performance that depends more on contact quality than solely on the thickness of the absorber layer [94-96]. Contact resistance is another major limitation, arising from poor energy

(This work is licensed under a Creative Commons Attribution 4.0 International License.)

International Journal of Engineering Research & Technology (IJERT)
ISSN: 2278-0181
Vol. 15 Issue 11 , November - 2026

compatibility, inadequate conductivity of the back electrode or the conductor layer, and the formation of a barrier at the interface [95-97]. Even a contact with moderate resistance can increase the series resistance (Rs), reduce the slope of the peak power curve (J_V) near the peak power point, and restrict current flow under operating conditions. In practical devices, the measured resistance is determined not only by the electrode resistance but also by the resistance of the interface, the conductor layer, and the current propagation path [95-97]. Therefore, the performance of a contact with high nominal conductivity may remain poor if the interface barrier is large or chemically unstable. Parasitic losses are closely related to these electrical limitations. These losses include recombination losses, resistive losses, and optical or chemical losses resulting from imperfect back contact materials [94–96]. For example, metallic electrodes may suffer from diffusion, interfacial reaction, or halide-induced corrosion, especially in halide-rich perovskite systems [98, 116-120]. These reactions lead to contact degradation, the formation of confined states, and accelerated long-term performance loss. In contrast, carbon-based and reduced graphene oxide contacts often offer better chemical stability, but their conductivity, work function, and interfacial quality are highly dependent on processing conditions [120–124, 98]. This means that stability improvements are not automatic; they must be balanced against transport and extraction efficiency. The situation becomes even more critical in lead-free systems such as tin-based perovskites. Due to Sn^{2+} oxidation, tin voids, and unintended p-type self-grafting, the absorber can already contain a high concentration of defects and free carriers [36–40]. Under these conditions, the back-end interface becomes highly sensitive to any additional disturbance. Even a slight increase in interface defect density or contact resistance can lead to a sharp drop in performance. Therefore, back-end contact geometry involves not only aligning energy levels but also suppressing recombination pathways and maintaining a chemically stable, low-resistance interface during operation [40, 93–97]. Numerical studies, particularly with SCAPS-1D, have shown that interface defect density, surface recombination velocity, contact occupancy function, and series resistance can significantly reshape the response of lead-free perovskite photovoltaic devices [90–92]. These models are useful because they separate the adsorbent effect from the contact effect. However, their predictive value depends on realistic assumptions about defect states, kinetics, and boundary conditions [90–92]. In practice, experimental interfaces are rarely perfect, so simulated performance should be interpreted as a limit, not a guarantee. In general, back contact losses in lead-free perovskite solar cells are subject to a combination of interfacial recombination, contact resistance, and chemical degradation. Therefore, successful back contact must perform functions beyond simply accumulating holes; it must also suppress recombination with the help of traps, reduce resistance, and maintain stability under thermal, electrical, and photostress [93-99]. For this reason, the next section on loss mechanisms should turn to material-specific back contact options and compare how different electrode classes cope with these constraints.

2 .2. SCAPS-1D as a Back Contact Design Tool

The SCAPS-1D software has become one of the most practical tools for studying thin-film solar cells prior to fabrication [125-128]. It enables researchers to test how the properties of the absorber material, defect density, interfacial states, contact work function, and transport layer parameters affect device performance. This software is particularly useful in back contact engineering, as the back interface is often difficult to isolate experimentally. SCAPS-1D helps to isolate the effect of resistivity in lead-free perovskite solar cells and surface defect loss. This is a critical point for lead-free and tin-based perovskite solar cells. These devices are highly affected by oxidation of tin(II) ions (Sn^{2+}), tin voids, and self-doping [36-40, 100-102]. Consequently, back contact can help to efficiently collect holes or increase recombination if the compatibility is poor. The SCAPS-1D software allows for the study of how changes in the work function, defect density, and contact selectivity affect voltage (Voc), short-circuit current density (Jsc), fill factor (F_F), and power conversion efficiency [125-128]. This provides a clearer picture of physically reasonable versus unreasonable contact designs. Another advantage of SCAPS-1D is its ability to evaluate different device configurations under the same assumptions. For example, noble metal contacts, carbon electrodes, and rGO-modified contacts can be compared while keeping the absorption and transport layers unchanged. This makes the comparison more consistent. It also helps determine whether performance improvements result from improved energy band alignment, reduced recombination, or simply lower series resistance. Of course, SCAPS-1D does not replace experimentation. The model's reliability depends on the accuracy of its inputs. Real-world interfaces may exhibit roughness, chemical interactions, diffusion, and irregular defects that are difficult to fully represent in one-dimensional simulations. Nevertheless, SCAPS-1D remains valuable because it provides a controlled method for testing design ideas and narrowing down research prior to fabrication [125-128].

(This work is licensed under a Creative Commons Attribution 4.0 International License.)

International Journal of Engineering Research & Technology (IJERT)
ISSN: 2278-0181
Vol. 15 Issue 11 , November - 2026

2.3. Numerical Insights into Contact Engineering

Numerical modeling provides a more direct way to understand why some back contacts outperform others [125-128]. In thin-film solar cells, performance is determined not only by the quality of the absorber material, but back contact also plays a key role through energy band alignment, contact resistance, and recombination at the interface. These effects are difficult to isolate experimentally, especially when multiple losses occur simultaneously. The SCAPS-1D software is useful because it allows these factors to be studied one by one. This is particularly important for lead-free tin perovskites. The absorber material already has a high defect density and is prone to oxidation and self-grafting [36-40, 100-102]. This means that the back contact must do more than simply conduct current; it must efficiently extract holes, avoid barrier formation, and limit recombination at the back interface. Numerical simulations can demonstrate the sensitivity of a device to the contact work function, charge trap density at the interface, and resistance loss due to imperfect contact layers. This type of analysis is also useful when comparing different contact materials. A highly conductive metal may exhibit poor performance if it forms a Schottky barrier or accelerates its degradation. Carbon and reduced graphene oxide (rGO) may appear less conductive in their solid state, but they can improve performance if they provide a more stable and compatible interface. The SCAPS-1D software helps to clarify this trade-off, highlighting that good contact geometry encompasses not only electrical conductivity but also interface quality, selectivity, and stability. The main limitation is the need to avoid over-interpreting numerical results, as simulated optimization does not guarantee the same outcome in a real device. Nevertheless, the model is very useful for identifying the most important design variables and for guiding experiments toward more realistic back-contact structures [125-128].

2.4. Numerical Modeling with SCAPS-1D

SCAPS-1D is a widely used one-dimensional numerical tool for analyzing thin-film solar cells, including lead-free perovskite devices. In previous studies, the software has been used to examine the effects of absorber properties, transport-layer parameters, defect states, interface recombination, contact work function, and electrical resistance on photovoltaic performance. Its calculations are based on the self-consistent solution of Poisson's equation and the electron and hole continuity equations within the drift-diffusion framework . The electrostatic potential across the device is described by Poisson's equation:

$$\frac{d^2\Psi(x)}{dx^2} = \frac{g}{\varepsilon_0 \varepsilon_r}\left[\mathrm{p(x)} - \mathrm{n(x)} + N_D - N_A + \rho_p - \rho_n\right] \quad (1)$$

Here, q represents the electron charge, ε_0 the vacuum permittivity, and ε_r the relative permittivity. n(x) and p(x) represent the electron and hole concentrations, respectively, while N_D and N_A denote the donor and acceptor impurity concentrations. Furthermore, ρ_n and ρ_p refer to the charge densities associated with states or defects present in the material. These are used to determine the distribution of the electric potential within the cell system based on the charge distribution therein [95, 100].

The carrier distributions are determined from the continuity equations [96, 100]:

$$\frac{\partial n}{\partial t} = \frac{1}{g}\frac{\partial J_n}{\partial x} + (G_n - R_n) \qquad (2)$$

$$\frac{\partial p}{\partial t} = \frac{1}{g}\frac{\partial J_p}{\partial x} + \left(G_p - R_p\right) \qquad (3)$$

where J_n and J_p denote the electron and hole current densities, respectively, while G represents the charge carrier generation rate and R the recombination rate. These equations illustrate how carrier concentrations are governed by the influence of light and the internal electric field.

The drift-diffusion equations, which describe the motion of electrons and holes under the influence of the electric field and concentration gradients, are given as follows [96, 100]:

(This work is licensed under a Creative Commons Attribution 4.0 International License.)

International Journal of Engineering Research & Technology (IJERT)
ISSN: 2278-0181
Vol. 15 Issue 11 , November - 2026

$$J_n = g\mu_n nE + gD_n \frac{\partial n}{\partial x} \qquad (4)$$

$$J_p = g\mu_p pE + gD_p \frac{\partial p}{\partial x} \qquad (5)$$

In these equations, un and up represent electron and hole mobilities, respectively, while D_n and D_p represent their respective diffusion coefficients.

the SCAPS-1D software calculates key solar cell performance parameters: open-circuit voltage (V_{oc}), short-circuit current density (J_{sc}), fill factor (F_F), and conversion efficiency (eta: η). These parameters are directly used to evaluate the performance quality of a solar cell and to compare different device structures.[100].

The fill factor (F_F) is calculated using the following relationship:

$$F_F = \frac{V_{mp} * J_{mp}}{V_{oc} * J_{sc}} = \frac{P_{max}}{V_{oc} * J_{sc}} \qquad (6)$$

Here, V_{mp} and J_{mp} represent the voltage and current density at the maximum power point, while V_{oc} denotes the open-circuit voltage and Jsc the short-circuit current density. The fill factor (F_F) is a crucial parameter, as it reflects the efficiency of power extraction from the solar cell; a higher F_F value generally indicates lower internal losses and improved transport and contact characteristics within the device. As for the solar cell efficiency, (eta: η), it is calculated using the following relationship:

$$\eta = \frac{V_{oc} * J_{sc} * F_F}{P_{in}} = \frac{P_{max}}{P_{in}} \qquad (7)$$

For rear-interface studies, the main value of SCAPS-1D is that selected parameters can be varied systematically under controlled assumptions. For example, previous studies have changed the back-contact work function, interface-defect density, absorber doping, transport-layer properties, and series resistance to evaluate their effects on band bending, carrier extraction, recombination, and device efficiency. This approach helps separate energetic losses from resistive and defect-related losses. However, SCAPS-1D describes an idealized one-dimensional device. Its predictions may not fully capture surface roughness, electrode porosity, pinholes, lateral nonuniformity, chemical reactions, metal diffusion, and time-dependent ion migration, [97, 100].

2 .5. Calibration of the Reference Solar Cell ($CsSnI_3$)

Before comparing alternative back-contact materials, the numerical model must be calibrated using a reliable reference device to ensure confident interpretation of the simulated trends [100]. In published studies on lead-free perovskites, CsSnI3 is used as a reference absorber due to its combination of a narrow band gap and relatively good charge-transfer properties, although its practical use is still limited by Sn2+ oxidation, defect formation, and its high sensitivity to interfacial recombination. For this reason, many studies have adopted CsSnI3-based planar devices as reference systems for calibrating SCAPS-1D before testing contact engineering strategies. The reference design studied here follows a conventional n-i-p scheme consisting of an indium tin oxide (ITO) front electrode, 150 n.m TiO2 and an electron transport layer, 330 nm CsSnI3, an absorber, 200 nm Spiro-OMeTAD hole transport layer, and a gold back conductor [98,99,100]. The researchers performed the simulation under the following standard conditions: 300 K, 100 mW cm^{-2}, and an AM 1.5G solar spectrum. The model parameters, particularly the series resistance (Rοs) and branch resistance (Rοsh), and the recombination-related quantities, were tuned to simulate the experimentally reported photovoltaic response as accurately as possible. The calibrated model showed excellent agreement with the experiment. [100], the simulated values for Voc, Jsc, fill factor, and power conversion efficiency were very close to the measured values, indicating that the numerical setup accurately represented the device's physical characteristics.

(This work is licensed under a Creative Commons Attribution 4.0 International License.)

International Journal of Engineering Research & Technology (IJERT)
ISSN: 2278-0181
Vol. 15 Issue 11 , November - 2026

2.6. Cell Structural Configuration

This review is based on a conventional n-i-p design, one of the most widely used configurations for lead-free perovskite solar cells. In this design, the transparent front electrode is made of indium tin oxide (ITO), while the back electrode is made of metallic gold (Au) in the reference state. The adsorbent is CsSnI3, positioned between the electron-transfer and hole layers to form the intrinsic region of the device. This configuration is consistent with published studies on lead-free perovskites, where device performance is significantly affected by the alignment of the adsorbent with charge-selective contact points[100]. In tin-based perovskites, such as CsSsI3 and CsSnI3, the interface design is critical because porous surfaces, oxidation, and ion migration can enhance recombination near the electrodes. Similar concerns have been raised in halide-mixed perovskites, such as $CsSn(I_{1-x}Br_x)$ and $CsSn(I_{1-x}Br_x)$, as shown in figures (1,2) where structural modification can improve band gap matching but may also introduce additional structural and ionic complexity. In double perovskites like $Cs_2AgBiBr_6$, a larger band gap and fewer defects make the interface geometry more important. Similarly, in spatially ordered systems like $Cs_3Sb_2I_9$ and Cs3Bi2I9, the inherent layered or zero-dimensional nature limits charge transport and increases the importance of selective contacts and optimizing the interface geometry. In the reference structure, the hole-transporting layer consists of Spiro-OMeTAD [99,100], while the electron-transporting side consists of a compact TiO_2 layer and a porous TiO_2 layer. The embedded titanium dioxide (TiO_2) layer acts primarily as an electron-blocking contact layer, as shown in figure 1, 2, while the porous titanium dioxide layer increases the interfacial contact area and aids in charge extraction. This multilayer design is commonly used for electron transport to minimize interfacial barriers and suppress recombination losses. Transport layer modeling: To more realistically represent the porous titanium dioxide layer, a gradient of material properties was introduced across its thickness. This method mimics the gradual transition from the material's adsorption surface to the titanium dioxide-bound region [100, 101]. It helps reproduce the imperfect interfacial behavior often observed in experiments. In SCAPS-based modeling, this gradient is useful because it provides a more realistic description of charge transport, energy band alignment, and defect-assisted recombination at the interface[100,101].

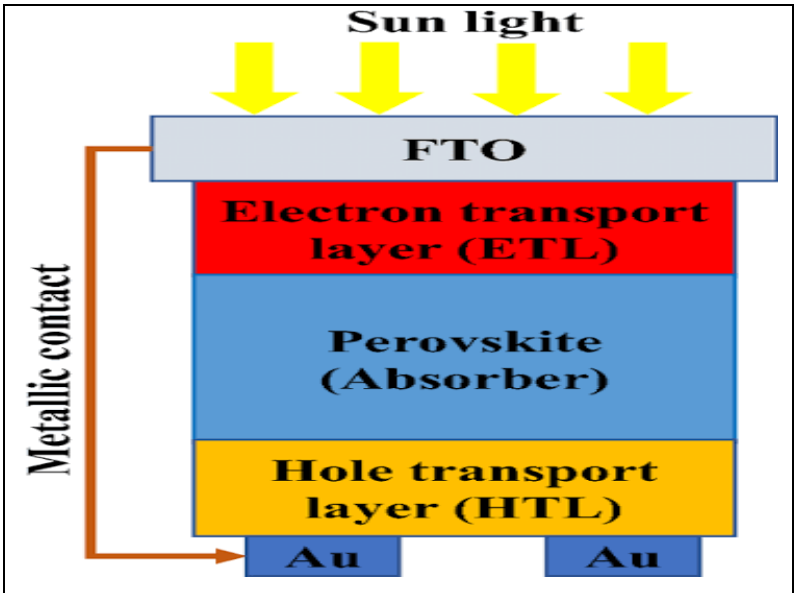


Fig. 1. Structure of the adopted solar cell.

(This work is licensed under a Creative Commons Attribution 4.0 International License.)

International Journal of Engineering Research & Technology (IJERT)
ISSN: 2278-0181
Vol. 15 Issue 11 , November - 2026

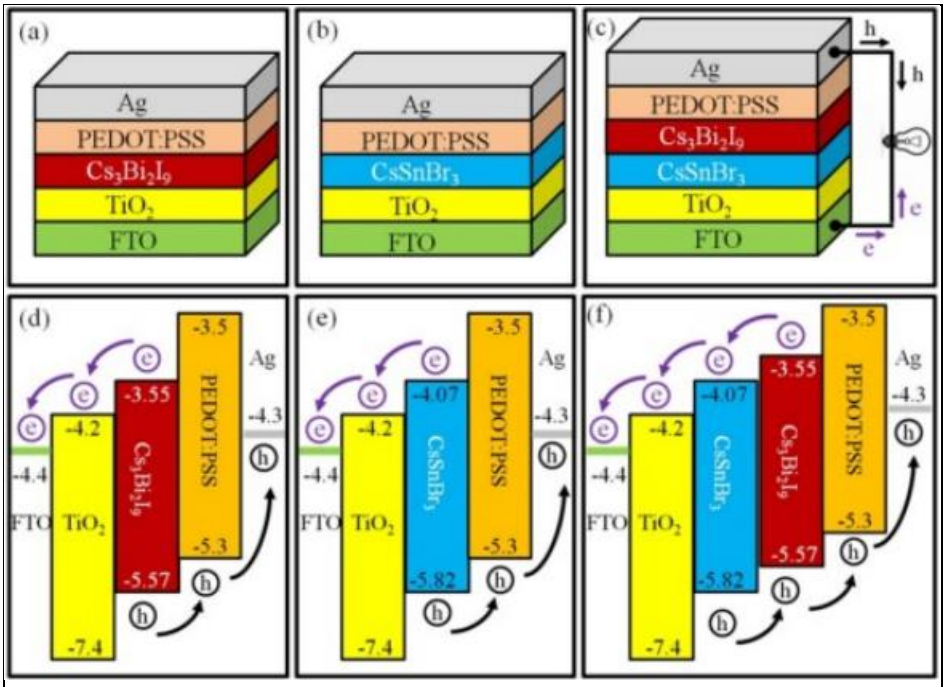


Fig.2. Solar cells based materiales (CsSnBr3/Cs3Bi2I9)[101]

2.7. Cell Operation Mechanism and Simulation Parameters

Upon exposure to light, the photons absorbed in the active layer generate electron-hole pairs. The separation and collection of these pairs depends on the internal electric field generated at the interfaces between the electron transport layer and the absorber layer, and between the absorber layer and the hole transport layer. Electrons migrate towards the electron-selective contact—typically TiO_2—while holes are extracted through the hole transport layer and ultimately collected at the back electrode [88,90,91]. The efficiency of this process is significantly influenced by the alignment of the energy bands, the kinetics of the charge carriers, the defect density (both within the material and at the interfaces), and the work function of the back contact. This general mechanism applies to the major groups of lead-free and perovskite-inspired sorbents discussed in this review: $FASnI_3$, $MASnI_3$, $CsSnBr_3$, the mixed-halide sorbent $CsSn(I_{1-x}Br_x)_3$, the double perovskite $Cs_2AgBiBr_6$, and the sterically arranged compounds $Cs_3Sb_2I_9$ and $Cs_3Bi_2I_9$. [34,37, 74,76]. However, the degree to which charge separation is achieved varies considerably among these materials. For tin-based iodide perovskites, specifically $FASnI_3$ and $MASnI_3$, the relatively narrow energy gaps and good charge carrier self-transport properties make them attractive sorbents. However, the oxidation of Sn^{2+} ions to Sn^{4+}, along with the formation of holes in the tin network, can lead to increased p-type self-doping and higher rates of non-radiative recombination. Therefore, efficient hole extraction and the provision of a chemically stable back contact are of particular importance in these cells. Using a back electrode with an unsuitable work function can lead to a barrier that hinders extraction and increases charge carrier accumulation near the hole transport layer, reducing both the fill factor and the open-circuit potential. In systems composed entirely of inorganic tin halides, such as $CsSnBr_3$ and $CsSn(I_{1-x}Br_x)_3$, bromide incorporation provides a practical pathway for adjusting the energy gap and can enhance the suitability of the adsorbent for applications requiring a wide energy gap or for tandem cell applications. Generally, increasing the bromine (Br) content leads to a wider energy gap; however, modifying the chemical composition can also alter the energy band positions, defect chemistry, and ionic behavior of the material. Therefore, the back-contact enhancement process is inextricably linked to the chosen iodine-to-bromine (I/Br) ratio. In these systems, the diffusion of the metal from the electrode and the migration of ions toward the interfaces can lead to the formation of recombination centers and accelerate the degradation of cell performance, making chemically inert electrodes or suitable buffer layers at the interfaces attractive alternatives to conventional metals. The issue of charge accumulation in materials such as $Cs_2AgBiBr_6$, $Cs_3Sb_2I_9$, and $Cs_3Bi_2I_9$ is of increasing importance and sensitivity[71,73,76] . Although these materials exhibit better environmental compatibility—and in many cases, higher oxidation resistance—than tin-based perovskites, their photovoltaic performance is often

(This work is licensed under a Creative Commons Attribution 4.0 International License.)

International Journal of Engineering Research & Technology (IJERT)
ISSN: 2278-0181
Vol. 15 Issue 11 , November - 2026

limited by a large energy gap, low charge carrier mobility, short diffusion distances, and defect-related recombination processes.[66,67, 69,70]. In $Cs_2AgBiBr_6$, indirect (or weakly allowed) phototransitions and a relatively large energy gap restrict photocurrent generation. For $Cs_3Sb_2I_9$ and $Cs_3Bi_2I_9$, their low-dimensional, spatially ordered crystal structures can further restrict charge carrier transport. Consequently, contact engineering is not merely a secondary step in improving these materials; it is essential for minimizing losses at the interfaces and enhancing charge extraction. In numerical simulations, the thickness of each layer should be chosen with a balance between light absorption and charge carrier transport. Increasing the thickness of the absorbing layer may enhance light absorption, but it may also increase the bulk recombination rate if the charge carrier diffusion distance is limited. This is particularly important for $Cs_2AgBiBr_6$, $Cs_3Sb_2I_9$, and $Cs_3Bi_2I_9$, where transport constraints are more pronounced than for $FASnI_3$ or $MASnI_3$.[73,76]. Therefore, a standardized device geometry can be used for comparative simulations, but the optimal thickness should be independently investigated for each absorbing material. In the reference configuration, the thickness of the absorbent material was set at 800 nm, while the thicknesses of the Spiro-OMeTAD, mesoporous TiO_2, and compact TiO_2 layers were set at 200 nm, 50 nm, and 100 nm, respectively. These values provide a consistent framework for comparing the effects of both the absorbent material composition and the back-contact [100, 102].

Table (1): Adopted physical properties and parameters of the layers used in the ($FASnI_3$, $MASnI_3$, $CsSnBr_3$, $Cs_2AgBiBr_6$, $Cs_3Sb_2I_9$, $Cs_3Bi_2I_9$, CsSnI3) -based perovskite solar cell.

hysical property	$FASnI_3$	$MASnI_3$	$CsSnBr_3$	$Cs_2AgBiBr_6$	$Cs_3Sb_2I_9$	$Cs_3Bi_2I_9$	Spiro-OMeTAD	($CsSnI_3$)	TiO_2	ITO
Thickness (nm)	350	500	500	500	800	500	200	800	150	500
Bandgap, Eg (eV)	1.41	1.3	1.7	2.05	1.95	2.03	3.00	1.27	3.20	3.50
Electron affinity χ (eV)	3.5	4.2	4.17	4.19	4.5	3.4	2.45	4.47	4.00	4.00
Relative permittivity, ε_r	8.2	10	9.9	5.8	4.19	9.68	3	18	9	9
Effective density of states in the conduction band, N_C (cm^{-3})	1×10^{18}	1×10^{18}	1×10^{19}	1×10^{16}	1×10^{18}	4.5×10^{19}	2.2×10^{18}	1.0×10^{19}	1.0×10^{2}	2.2×10^{1}
Effective density of states in the valence band, N_V(cm^{-3})	1×10^{18}	1×10^{18}	1×10^{18}	1×10^{16}	2.4×10^{19}	2×10^{19}	1.9×10^{19}	1.0×10^{19}	2.0×10^{2}	2.2×10^{1}
Electron mobility μ_n ($cm^2.V^{-1}.s$	22	1.6	15	11.81	11.3	4.3	2.0×10^{-4}	4.37	20	20
Hole mobility,	22	1.6	5.8	0.49	5.58	1.7		4.37	10	10

(This work is licensed under a Creative Commons Attribution 4.0 International License.)

International Journal of Engineering Research & Technology (IJERT)
ISSN: 2278-0181
Vol. 15 Issue 11 , November - 2026

$\mu_p\ (cm^2.V^{-1}.s$							2.0×10^{-4}			
Acceptor concentration , $N_A(cm^{-3})$	7×10^{16}	1×10^{15}	1×10^{18}	1×10^{15}	1×10^{15}	1×10^{15}	2.0×10^{18}	1.8×10^{16}	0	0
Donor concentration , $N_D(cm^{-3})$	0	0	0	0	0	0	0	0	5.0×10^{1}	1.0×10^{2}
Defect/trap concentration , $N_T(cm^{-3})$	2×10^{15}	1×10^{14}	1×10^{15}	1×10^{15}	1×10^{14}	1×10^{14}	1.0×10^{15}	1.0×10^{13}	1.0×10^{1}	1.0×10^{1}

Device Architecture, Loss Mechanisms, and Back-Contact Models: A Comparative Review

In the field of numerical simulation and interface modeling for lead-free perovskite solar cells (PSCs), establishing realistic baseline parameters is crucial for generating reliable predictive trends. Study [106] established a prominent reference model by accounting for discrete interfacial defect states at heterojunction boundaries and calibrating the resulting electrical characteristics against experimental device data. However, as recent studies indicate, previous modeling frameworks often relied on simplified physical approximations—such as limiting analysis to the Shockley-Read-Hall (SRH) recombination model, employing an idealized single-layer electron transport layer (ETL), or restricting the scope to a single light-absorbing material composition [104-106]. To develop a comprehensive comparative perspective, it is essential to systematically evaluate physical loss mechanisms and contact engineering models across diverse families of lead-free absorbers.

3. RECOMBINATION DYNAMICS AND PHYSICAL TRANSPORT MODELS

While early simulation studies primarily assessed device losses through trap-assisted bulk recombination (SRH), recent research emphasizes that systems characterized by high charge-carrier densities and narrow bandgaps necessitate the inclusion of direct band-to-band (radiative) recombination and three-particle (Auger) recombination processes . The relative contribution of these recombination pathways varies significantly across lead-free perovskite systems:

Tin-based halide perovskites (e.g., $FASnI_3$, $MASnI_3$, $CsSnBr_3$, and $CsSn(I_{1-x}Br_x)_3$): As reported in multiple studies (e.g), tin (Sn)-based absorbers exhibit high intrinsic background charge-carrier densities (ranging from 10^{16} to 10^{18} cm^{-3}); this stems from the spontaneous oxidation of Sn^{2+} ions to Sn^{4+} and the low formation energy of tin vacancies (Sn-vacancies) [10-111]. Consequently, Shockley-Read-Hall (SRH) recombination within the bulk—coupled with significant Auger losses near interfaces—dominates device performance degradation, necessitating precise calibration of both defect cross-sections and carrier lifetimes. Double perovskites and vacancy-ordered halide structures (e.g., $Cs_2AgBiBr_6$, $Cs_3Sb_2I_9$, and $Cs_3Bi_2I_9$): In contrast, studies by Slavney et al. [108] and subsequent simulation reports [107,112] highlight that these configurations—characterized by wider bandgaps and reduced dimensionality—suffer primarily from low charge-carrier mobility ($\mu < 10$ cm^2 V^{-1} s^{-1}), short carrier diffusion lengths, and the presence of localized trap states. In these systems, interface-induced Shockley-Read-Hall (SRH) recombination is the primary limiting factor, rendering the charge-carrier collection process highly sensitive to the spatial distribution of electric fields at the interfaces.[111,114].

(This work is licensed under a Creative Commons Attribution 4.0 International License.)

International Journal of Engineering Research & Technology (IJERT)
ISSN: 2278-0181
Vol. 15 Issue 11 , November - 2026

3.1. Front-contact engineering and electron transport:

Bilayer vs. monolayer TiO_2 configurations. A recurring shortcoming in previous perovskite simulation studies is the representation of the front contact as a simple, planar TiO_2 monolayer [113]. Advanced experimental and numerical studies demonstrate that a bilayer electron-transport structure—combining a compact blocking layer (c-TiO_2) with a mesoporous structure (m-TiO_2)—provides a more realistic representation of high-efficiency designs [113]: c-TiO_2 layer (approx. 50–100 nm): Primarily acts as a physical, pinhole-free barrier to prevent direct shunting between the transparent conductive oxide (FTO/ITO) layer and the light-absorbing perovskite material[100,114]. m-TiO_2 layer (approx. 50–150 nm): Permeated by the perovskite absorber, this layer increases the interfacial heterojunction area, shortens the required electron diffusion path, and minimizes charge accumulation near the front interface. Explicitly accounting for the effective dielectric constant, porosity-dependent mobility, and interfacial defect distributions in both layers (c-TiO_2 and m-TiO_2) resolves the discrepancies often observed between idealized one-dimensional (1D) planar models and experimental current-voltage (J–V) characteristics. [113,114].

3.2. Back Contact Selection: Noble Metals vs. Low-Cost Alternatives

Selecting the back electrode involves a critical and delicate balancing act between ohmic hole extraction, chemical stability, and industrial manufacturing costs. Although gold (Au) remains the standard reference electrode—owing to its suitable work function ($\Phi \approx 5.1$ eV) and the minimization of the Schottky barrier at the interface between the hole transport layer (HTL) and the electrode [100]—its high cost and tendency to diffuse into the active layer limit its potential for widespread commercialization.

Numerous research groups—spanning both experimental and modeling disciplines—have investigated earth-abundant material alternatives, revealing distinct trade-offs depending on the material employed.[100].

3.3. Carbon-based electrodes (graphite, carbon black, graphene):

Studies [115- 118] have shown that carbon contacts possess an effective work function of approximately 5.0 eV—a value very close to that of gold (Au)—while offering chemical inertness that prevents the migration of halides and tin. In tin-based systems (such as $FASnI_3$ and $CsSnI_3$), carbon back contacts significantly retard oxidation—whether caused by the ambient environment or the electrode itself—thereby providing a practical pathway toward the production of low-cost or hole-transport-layer-free (HTL-free) commercial modules [116- 118].

3.4. Transition metals (Ni, Cu, Ag):

Comparative studies [119, 120] highlight nickel ($\Phi \approx 5.04$ eV) as an effective metallic alternative to gold, owing to its high work function. In contrast, metals with lower work functions such as silver (Ag, $\Phi \approx 4.26$ eV) and copper (Cu, $\Phi \approx 4.65$ eV) result in the formation of a significant Schottky extraction barrier. Furthermore, copper and silver are prone to reacting with halogens (such as the formation of AgI or CuIx), which accelerates interface degradation unless they are protected (passivated) by dense insulating layers.[122,121].

3.5. Absorber material compatibility:

For tin-based perovskites (Sn-based perovskites), contact architecture must prioritize preventing the ingress of metal ions, which exacerbates the formation of tin vacancies (Sn vacancies) [123,108]. For materials such as $Cs_2AgBiBr_6$, $Cs_3Sb_2I_9$, and $Cs_3Bi_2I_9$—where low charge-carrier mobility already hinders carrier collection—the presence of a moderate extraction barrier at the contact ($\Delta\Phi > 0.3$ eV) leads to a sharp reduction in both open-circuit voltage (Voc) and fill factor (F_F).[111,124- 127].

4. EXPERIMENTAL STUDIES ON BACK-CONTACT ENGINEERING IN LEAD-FREE PEROVSKITE SOLAR CELL

4.1. Photovoltaic performance of gold (Au) back contact solar cell

Based on the reference model featuring a gold (Au) back contact,[100] numerical simulations performed using SCAPS-1D showed the following values for the photovoltaic parameters: Open circuit voltage (V_{OC}): 0.886V; Short-short current density (J_{SC}) = 31.85 mA/cm^2; Fill factor (FF) = 61.67%, Power conversion

(This work is licensed under a Creative Commons Attribution 4.0 International License.)

International Journal of Engineering Research & Technology (IJERT)
ISSN: 2278-0181
Vol. 15 Issue 11 , November - 2026

efficiency $(\eta) = 17.42\%$.These parameters indicate strong device performance with high optical absorption and high quantum yield, especially in the spectral range above 400 nm.[100], The alignment of the energy beams at the interfaces is also highly ideal, thanks to the smooth gradient in physical properties, particularly within the porous titanium dioxide $(m - TiO_2)$ layer. The corresponding device characteristics are shown in the figures below: Figure 3 shows the current density versus voltage (J-V) curve, Figure 4 displays the quantum efficiency (QE) spectrum as a function of wavelength, while Figure 5 shows the energy band diagram showing the alignment of valence bands and conduction across the device structure[100].

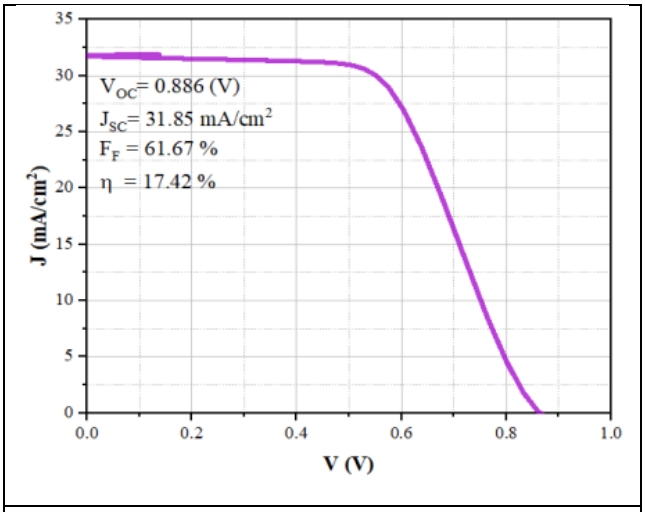


Fig.(3) J-V diagram of the basic solar cell [100]

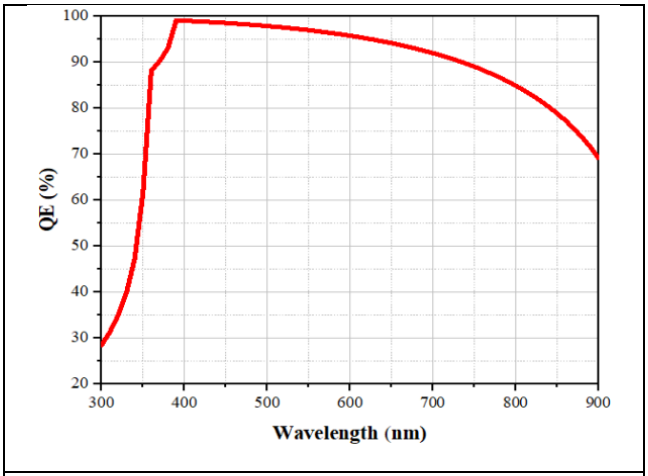


Fig. (4): Quantum yield (QE) as a function of wavelength for the basic solar cell [100]

4.1.1. Effect of the Back Contact Layer:

The back contact layer is a critical component in solar cell design, as it fundamentally dictates the photovoltaic properties and overall device efficiency. It regulates charge extraction and transport, minimizes series resistance, and ensures high interface quality with the absorber layer, thereby reducing energy barriers [128]. In this study, Gold (Au) was employed as the baseline back contact due to its excellent electrical characteristics, including a high work function (~5.1 eV), superior chemical stability, and the formation of an ideal Ohmic contact with the perovskite absorber . However, the high cost of gold presents a significant barrier to commercial scalability. Consequently, there is an urgent need to investigate cost-effective alternatives that can deliver comparable performance. Several economic metallic alternatives were evaluated, taking into account their respective work functions, as summarized in Table 2 [128 ,133].

(This work is licensed under a Creative Commons Attribution 4.0 International License.)

International Journal of Engineering Research & Technology (IJERT)
ISSN: 2278-0181
Vol. 15 Issue 11 , November - 2026

Table (2): Work function values for the evaluated metals [100]

Material	Work Function Φ (eV)
Al	4.41
Cr	4.50
Cu	4.65
Ag	4.71
Fe	4.81
rGO	4.90
C–Mo	5.00
Ni	5.15
W	5.22

It can be incorporated into the text as follows: Table 2 lists the work function values of the studied materials, which range from (4.41) to (5.22) eV. Among these materials, Al exhibits the lowest work function, whereas W shows the highest value. Au was considered as the reference back contact, with a work function of approximately (5.1) eV. Variations in work function play a key role in determining energy band alignment and the quality of interfacial contact with the absorber layer, thereby influencing the suitability of each material as a back contact in the solar cell.

4.2. Carbon/Graphene-Based Hybrid Back Contacts

Bedicode, Simal, and Statatus (2021)[144] reviewed the use of carbon back electrodes in low-toxicity, lead-free perovskite solar cells (LF-PSCs), with a particular focus on tin-based, bismuth-based, and bi-perovskite materials. Carbon electrodes are attractive not only because of their lower cost compared to precious metals like gold and silver, but also because they offer several chemical and surface advantages that help mitigate common degradation mechanisms in LF-PSCs. The carbon work potential is approximately ΦC ≈ 5.0 eV, which is close to that of gold (ΦAu ≈ 5.1 eV). Carbon's relatively high work function allows for a favorable energy level match with the valence band maximum (VBM) of many lead-free absorber perovskites and with the highest occupied molecular orbital (HOMO) of organic and inorganic hole-transfer layers (HTLs). This suitability facilitates hole extraction and reduces the hole extraction barrier (ΦB,h) at the back surface. Another important advantage of carbon is its relatively high chemical stability. Unlike conventional metal conductors, carbon is less susceptible to metal ion migration and halide-induced corrosion, which can negatively affect gold and silver electrodes. Furthermore, carbon's hydrophobic nature provides protection against moisture penetration, helping to slow degradation from environmental exposure. These properties are particularly important for tin perovskites such as $MASnI_3$, $FASnI_3$, and $CsSnI_3$. These materials are highly sensitive to the oxidation of tin(II) ions (Sn^{2+}) to tin(IV) ions (Sn^{4+}) and often suffer from high back carrier concentrations due to p-type self-doping and large non-radiative recombination. Researchers have reported that using carbon electrodes with tin halide perovskites, including $MASnIBr_{1.8}Cl_{0.2}$ and a two-dimensional dione-Jacobson $(4AMP)(FA)_3Sn_4I_{13}$ structure, resulted in power conversion efficiencies of approximately 3.1% to 4.22% in low-temperature hole-transfer layer (HTM)-free devices. As shown in figure(5).[134].

(This work is licensed under a Creative Commons Attribution 4.0 International License.)

International Journal of Engineering Research & Technology (IJERT)
ISSN: 2278-0181
Vol. 15 Issue 11 , November - 2026

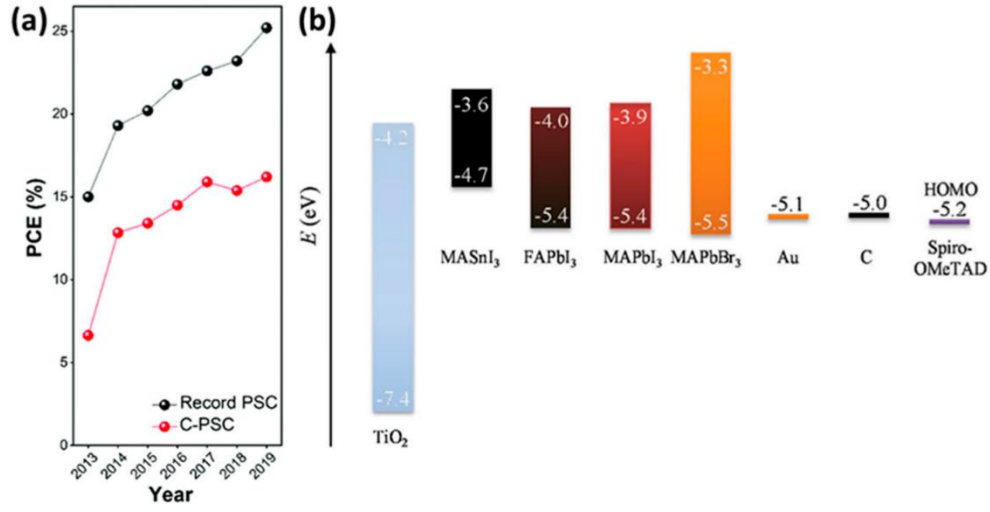


Figure 5: (a) Summary of development in PCEs of C-PSCs in comparison to state-of-the-art PSCs . Reproduced with permission Copyright 2020 Royal Society of Chemistry. (b) schematic energy level diagram of perovskite materials, TiO2, Spiro-OMeTAD, Au and C .[134].

These devices also exhibited improved stability under ambient and illumination conditions compared to some devices using conventional metal conductors. Carbon electrodes have also been investigated in lead-free double perovskites. For example, devices based on lithium-ion-doped $Cs_2AgBiBr_6$ crystals and carbon back electrodes achieved a stable energy conversion efficiency of approximately 2.57%. More importantly, these devices exhibited good thermal stability, maintaining their operational performance for over 90[144]. days at 25 °C and for approximately 60 days under unencapsulated thermal stress at 85 °C. Despite these advantages, pure carbon electrodes still suffer from some limitations related to charge transport. Conventional graphite and carbon black pastes generally have moderate electrical conductivity and relatively high surface resistivity. Furthermore, the physical contact between the carbon electrode and the perovskite absorber or pore-transfer layer may not be sufficiently homogeneous at the microscopic level. These limitations can increase the series resistivity (Rs) of the device, thereby reducing the fill factor (FF). One approach to overcoming these limitations is to combine carbon materials with low-dimensional carbon nanomaterials, such as graphene, reduced graphene oxide (rGO), and carbon nanotubes (CNTs). These nanomaterials can form a more cohesive conductive network, improve charge transport, and reduce microscopic gaps at the interface. They can also help modify the interface dipole and fine-tune the effective work function of the carbon electrode. Therefore, developing carbon back electrodes for lead-free perovskite solar cells should not be considered simply a replacement for precious metal interconnects; it requires a comprehensive interface engineering strategy. This strategy must simultaneously address energy level alignment, contact resistance, interface defects, and long-term chemical stability. Such an approach would make carbon electrodes a low-cost, chemically stable, and environmentally attractive option for developing the next generation of low-toxicity perovskite solar cells. In addition to the inherent photovoltaic properties of carbon materials, the overall electrical and mechanical performance of carbon back electrodes is significantly influenced by the composition and curing method of the carbon paste. Specifically, the choice of polymer binder, the paste's flow properties, and its solvent compatibility can significantly affect the quality of the electrode-hole transport layer (HTL). Forouzandeh et al. (**2024**)[135] investigated these effects by comparing three polymer binders—poly(methyl methacrylate) (PMMA), ethyl cellulose (EC), and styrene-butadiene-styrene (SBS)—with an inorganic, impurity-free, oleamine-coated $CuInS_2$ nanoparticle-based HTL. Their results demonstrated that efficient charge extraction is determined not only by the electrical resistivity (ρ) of the carbon electrode but also by the quality of the physical contact between the electrode and the HTL. Good interfacing and mechanical stability are essential for minimizing contact resistance (R_contact) and preventing cracking or segregation under mechanical and thermal stresses. Among the tested formulations, the PMMA-based carbon paste exhibited the lowest specific resistance, $\rho = 0.0473\ \Omega\cdot cm$. However, its relative brittleness led to micro-crack formation and eventual segregation at the interface. These

(This work is licensed under a Creative Commons Attribution 4.0 International License.)

International Journal of Engineering Research & Technology (IJERT)
ISSN: 2278-0181
Vol. 15 Issue 11 , November - 2026

defects increased the electrical resistivity and negatively impacted the fill factor (FF). In contrast, the SBS rubber bond provided greater flexibility and mechanical strength, allowing the graphite flakes and carbon black particles to form a more stable and continuous conductive network. The SBS-based electrode maintained good contact with the underlying $CuInS_2$ hole-transfer layer and demonstrated excellent mechanical toughness, withstanding over 1000 continuous bending cycles without significant deterioration in electrical or structural properties. As shown in figure(6), [135].

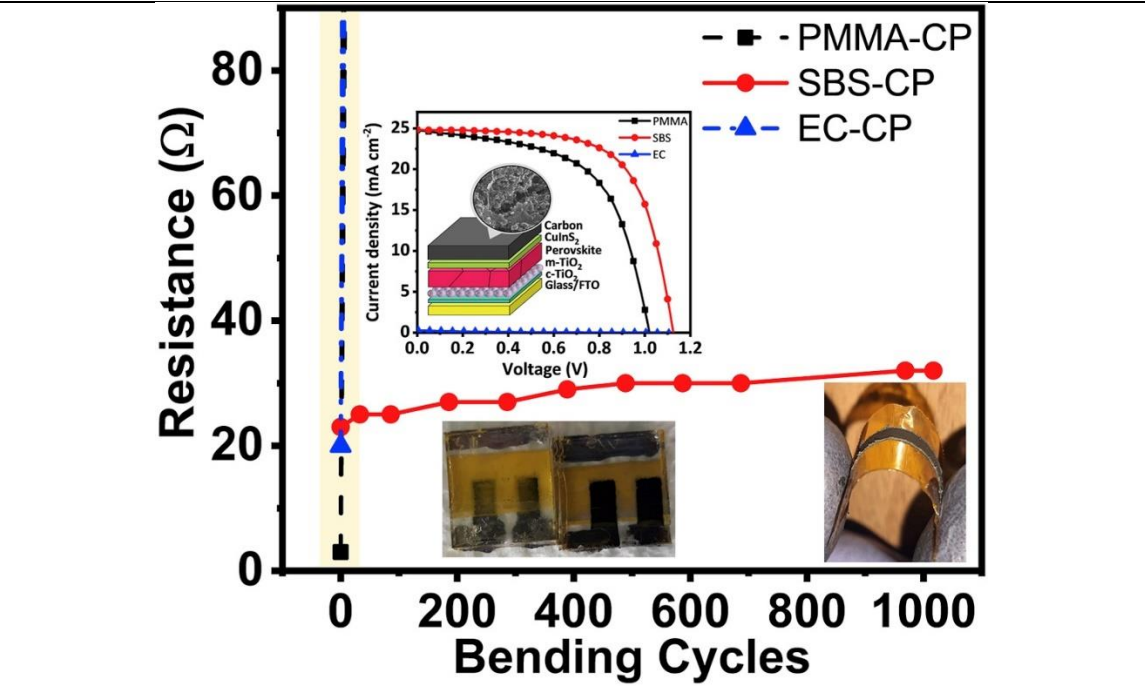


Figure (6): Electrical and photovoltaic response of the carbon-based back-contact electrodes under repeated bending. The PMMA-based carbon paste (PMMA-CP) exhibits the lowest initial resistance but undergoes severe mechanical failure, whereas the EC-based electrode (EC-CP) shows poor mechanical integrity and becomes discontinuous. In contrast, the SBS-based carbon paste (SBS-CP) maintains a relatively stable resistance throughout more than 1000 bending cycles, indicating superior flexibility, adhesion, and structural integrity. The inset presents the corresponding J–V characteristics of the devices, together with the schematic device architecture and representative photographs before and after bending. The results demonstrate that mechanical robustness and interfacial continuity, rather than initial bulk conductivity alone, are critical parameters for reliable carbon back-contact electrodes in perovskite solar cells[135]

The improved interfacial contact provided by the SBS formulation resulted in reduced interfacial voids and a decrease in total series resistance (Rs). Consequently, the corresponding devices achieved a peak power conversion efficiency (PCE) of 18.6%. In addition to the electrical improvement, the combination of the hydrophobic $CuInS_2$ hole-transfer layer and the dense, chemically stable carbon electrode provided robust protection against environmental degradation. The devices maintained stable operation for approximately 172 days at 40% relative humidity without packaging, demonstrating the potential of this electrode design to enhance long-term device stability. These results provide valuable guidance for the design of carbon back-conductors in lead-free perovskite solar cells (LF-PSCs). Lead-free adsorbent materials, particularly Sn^{2+}-based perovskites and bismuth-based double perovskites, are highly sensitive to humidity, solvent exposure, and defects at the interfacial surfaces. Therefore, the back electrode should be carefully designed to avoid any chemical or structural damage during deposition, while maintaining compatibility with low-temperature processing. One of the study's key findings is that optimizing the polymer-solvent bonding system is just as important as selecting a suitable carbon-based conductive filler. A suitable bonder can improve the mechanical integrity of the back link, reduce interfacial defects, and maintain stable contact with the underlying transport layer. This, in turn, helps minimize trap formation and supports continuous charge carrier extraction, while preserving the chemical and structural integrity of the photosensitive layers.

(This work is licensed under a Creative Commons Attribution 4.0 International License.)

International Journal of Engineering Research & Technology (IJERT)
ISSN: 2278-0181
Vol. 15 Issue 11 , November - 2026

Accordingly, optimizing the carbon electrode in low-temperature photovoltaic solar cells should consider the entire electrode structure, rather than focusing solely on the electrical conductivity of the carbon filler.[135].

the latest developments in transparent conductive materials for photovoltaic applications, with a particular focus on graphene and carbon nanotube networks. Although their study did not specifically focus on lead-free perovskite solar cells, the physical principles discussed are highly relevant to the development of hybrid back-conductors based on graphene and carbon nanotubes. Graphene is an attractive electrode material due to its high electrical conductivity, low surface resistance, optical transparency, and excellent chemical, thermal, and mechanical stability. These properties make it suitable for improving upon or partially replacing conventional metal electrodes and carbon nanotubes. However, the use of graphene requires a delicate balance between electrical conductivity and optical transparency. Increasing the number of graphene layers generally reduces surface resistance but also reduces the amount of light transmitted through the film. Each additional graphene layer reduces optical transmittance by approximately 2.3%. Therefore, the thickness of the graphene should be carefully optimized rather than simply increased to achieve higher conductivity.

The optimal thickness must provide sufficient electrical transfer while minimizing light loss and ensuring adequate coverage of the lower interface. The electrical properties of graphene can also be modified through p-type chemical or molecular doping. Doping materials such as MoO_3, HNO_3, HCl, and $AuCl_3$ can alter the Fermi level, increase the hole concentration, and modify the effective work function of the graphene electrode. Appropriately modifying the work function can improve the compatibility of energy levels with the highest occupied energy level (HOMO) of the hole-transfer layer, facilitating hole extraction and reducing charge accumulation at the interface. This approach is particularly important for lead-free perovskite solar cells, as tin- and bismuth-based adsorbents can be severely affected by surface defects and non-radiative recombination. Therefore, the effectiveness of graphene in hybrid back-contacts should be evaluated not only by its conductivity but also by its work function, surface dipole, defect density, and chemical compatibility with the adjacent hole-transfer material. [145]. As figure(7)

(This work is licensed under a Creative Commons Attribution 4.0 International License.)

International Journal of Engineering Research & Technology (IJERT)
ISSN: 2278-0181
Vol. 15 Issue 11 , November - 2026

Device Architecture	FF (%)	PCE
Glass/AgNWs-G1/SnO_2/Perovskite/Carbon [39]	43.64	10
Glass/AgNWs-G2/SnO_2/Perovskite/Carbon [39]	66.46	15
Glass/G-2(HNO_3-doped)/PEDOT:PSS/n-Si/LiF/Al [36]	40	5.
Glass/G-3(HNO_3-doped)/PEDOT:PSS/n-Si/LiF/Al [36]	39	5.
Glass/G-4(HNO_3-doped)/PEDOT:PSS/n-Si/LiF/Al [36]	47	5.
Glass/G-3(undoped)/PEDOT:PSS/n-Si/LiF/Al [36]	36	3.
Glass/G-3(undoped)-(1 month)/PEDOT:PSS/n-Si/LiF/Al [36]	38	4.
Glass/FTO/Compact-TiO_2/$MAPbI_{3-x}Cl_x$/Spiro-OMeTAD/PEDOT:PSS/G-1 [169,176]	59.07	8.
Glass/FTO/Compact-TiO_2/$MAPbI_{3-x}Cl_x$/Spiro-OMeTAD/PEDOT:PSS/G-2 [169,176]	71.72	12
Glass/FTO/Compact-TiO_2/$MAPbI_{3-x}Cl_x$/Spiro-OMeTAD/PEDOT:PSS/G-3 [169,176]	67.58	10
Glass/FTO/Compact-TiO_2/$MAPbI_{3-x}Cl_x$/Spiro-OMeTAD/PEDOT:PSS/G-4 [176]	68.37	10
Glass/Graphene/MoO_3-1 nm/PEDOT:PSS/Perovskite/C60/BCP/LiF/Al [170]	45	6
Glass/Graphene/MoO_3-2 nm/PEDOT:PSS/Perovskite/C60/BCP/LiF/Al [170]	72	16
Glass/Graphene/MoO_3-4 nm/PEDOT:PSS/Perovskite/C60/BCP/LiF/Al [170]	70	15
G-3/MoO_3+PEDOT:PSS/P3HT:PCBM/LiF/Al (HCl interlayer and HNO_3 doping) [191]	45	1
Graphene/PEDOT:PSS/P3HT:PCBM/LiF/Al [191]	51	2
Glass/SnO_2:F/TiO_2/$CH_3NH_3PbI_3$/spiro-OMeTAD/graphene [192]	56.6	8
PET/APTES/$AuCl_3$-G/PEDOT:PSS/$FAPbI_{3-x}Br_x$/PCBM/Al [193]	76.2	17

Figure (7): A summary of the literature on transparent electrodes made of carbon materials used in solar cells.[135].

Carbon nanotubes offer another effective strategy for improving carbon back-connections. Their one-dimensional structure allows for the formation of conductive pathways between graphite flakes, carbon black particles, and areas where physical contact with the electrode may be incomplete. These interconnected pathways enhance charge transport and reduce localized contact resistance at the contact surface between the hole-transport layer and the electrode. Additionally, the relatively hydrophobic nature of carbon nanotube surfaces helps limit moisture penetration into the underlying perovskite layer. However, the electrical performance of carbon nanotube networks is highly dependent on their permeability behavior and layer thickness. Increasing the carbon nanotube content or layer thickness generally improves electrical conductivity, but excessive thickness can reduce optical transparency. Surface functionalization presents another challenge. While chemical treatment improves the dispersion and adhesion of carbon nanotubes to surrounding materials, the introduction of oxygen-containing functional groups may reduce the self-conductivity of the carbon nanotube network. Therefore, both the concentration of carbon nanotubes and the type of surface treatment must be precisely controlled. Reported results for carbon nanotube modification underscore the importance of interfacial control. For example, treating double-walled carbon nanotubes with trifluoromethanesulfonic acid (TFMA) improved their energy compatibility with PTAA, increasing the device efficiency from 14.4% to 16.0% and ensuring stability for over 100 days. Conversely, excessive MoO_3 layer thickness or improper treatment with nitric acid (HNO_3) resulted in energy level mismatch and a decrease in efficiency from 12.8% to 11.0%. These results indicate that carbon nanotube doping does not

(This work is licensed under a Creative Commons Attribution 4.0 International License.)

International Journal of Engineering Research & Technology (IJERT)
ISSN: 2278-0181
Vol. 15 Issue 11 , November - 2026

automatically improve photovoltaic performance; rather, its effectiveness depends on several factors, including the doping concentration, the formation of a dipole at the interfacial, the layer thickness, work function compatibility, and the chemical stability of the modified electrode. In general, graphene/carbon nanotube hybrid conductors offer several advantages over conventional carbon electrodes, including additional conduction pathways, work function modification, improved surface contact, and a degree of water resistance. However, their use in lead-free perovskite solar cells requires careful optimization, as improving one property may negatively impact another. Therefore, electrical conductivity, optical transparency, wettability, defect passivation, and long-term chemical stability must be considered holistically.

An study In (2025) used SCAPS-1D simulations to study a lead-free, hole-transfer-layer (HTL) perovskite solar cell with an FTO/TiO_2/IDL/$MASnI_3$/carbon architecture. This architecture is particularly relevant for carbon back-contact design because the carbon electrode is directly responsible for hole extraction and collection without the need for an additional hole-transfer layer. Under optimized conditions, the simulated device achieved a peak power conversion efficiency (PCE) of 22.23%, with an open-circuit voltage (V_oc) of 0.886 V, a short-circuit current density (J_sc) of 30.68 mA/cm², and a fill factor (FF) of 81.58%. The relatively high expected efficiency is primarily due to the optimal energy level compatibility between the maximum valence band of $MASnI_3$, located at approximately -4.8 eV, and the carbon work function, estimated at around 5.0 eV. This compatibility reduces the energy barrier required for hole extraction and allows for the formation of a quasi-ohmic bond at the back surface. Consequently, efficient hole collection can be achieved without the need for an additional hole-transfer layer, simplifying the device structure and reducing the number of interfaces. Furthermore, a comparison of the work functions of different back electrodes has shown that metals with low work functions, such as silver (4.74 eV) and iron (4.81 eV), are more likely to present an extraction barrier at the contact surface between $MASnI_3$ and the electrode. In contrast, carbon offers an ideal balance between suitable energy level compatibility, low cost, and chemical stability, eliminating the need for expensive metals with high work functions, such as platinum. This observation is particularly relevant for the development of graphene-modified carbon electrodes and carbon nanotubes. The addition of carbon nanomaterials should either maintain or appropriately modify the electrode's effective work function towards the valence band edge of the $MASnI_3$ compound, while simultaneously improving the back-junction conductivity. Therefore, the performance of the hybrid carbon electrode cannot be evaluated solely based on its overall electrical conductivity; the position of the Fermi level and the interpolar dipole also play a crucial role in determining hole extraction efficiency and back-junction quality. Simulations also highlighted the significant impact of parasitic series resistance on device performance. As the series resistance increased from 0 to 6 Ω·cm², the fill factor decreased from 78.6% to 64.49%, and the power conversion efficiency dropped from 21.41% to 17.4%. as shown in figure(8) This result underscores the importance of minimizing resistance within carbon back electrodes. Integrating graphene sheets or carbon nanotubes into conventional carbon electrodes may be an effective approach, as these nanostructures enable additional conduction pathways between the graphite and the carbon black molecules. They may also improve the microscopic coverage of the interface, reducing layer resistance and localized contact resistance. Simultaneously, simulations identified the contact surface between $MASnI_3$ and carbon as a potential region for increased recombination. Therefore, graphene/carbon nanotube integration should not only reduce Rs but also engineer the contact surface to minimize trap density, reduce unwanted electron transfer to the back electrode, and maintain selective hole extraction. This is particularly important for tin perovskites, where interface defects can lead to a significant increase in non-radiative recombination.[135].

(This work is licensed under a Creative Commons Attribution 4.0 International License.)

International Journal of Engineering Research & Technology (IJERT)
ISSN: 2278-0181
Vol. 15 Issue 11 , November - 2026

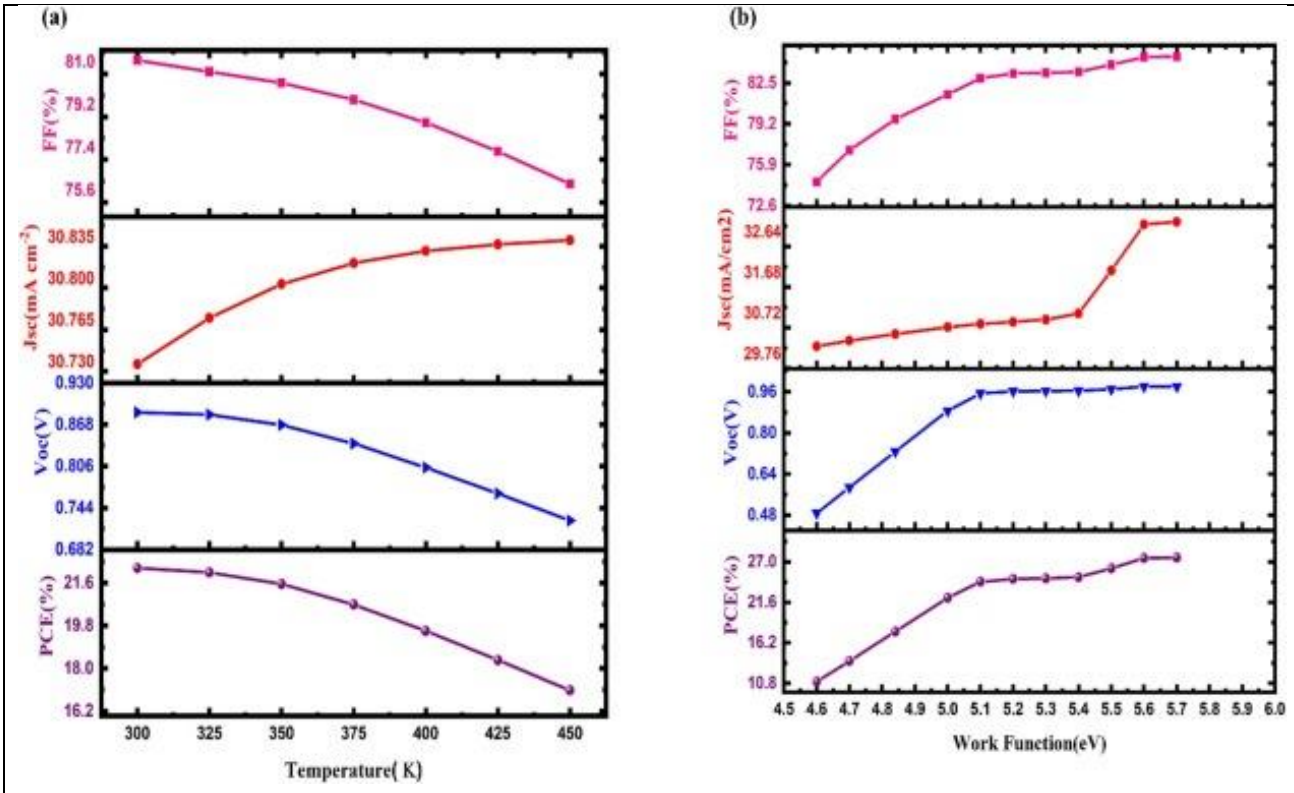


Fig. (8): Effect of (a) Temperature Changes and (b) Work Function on J-V Characteristics.

Despite the promising efficiency predicted by the simulations, these results should be considered an ideal theoretical benchmark, not a direct representation of experimental device performance. The model assumes optimized properties of the adsorbent material and contact surface, including a relatively low defect density of approximately 10^{13} cm^{-3}. In practical tin-based perovskites, Sn^{2+} oxidation to Sn^{4+}, p-type self-grafting, and a relatively high defect density can significantly affect charge transport and recombination. Furthermore, the carbon electrode in the simulation is primarily described by its occupation function and limiting electrical conditions. Important practical factors such as paste porosity, carbon nanodispersion, bonding material resistance, surface roughness, and potential chemical reactions at the back interface are not explicitly considered. Therefore, this study provides a useful theoretical reference for designing hybrid carbon/graphene back conductors for lead-free, tin-based perovskite solar cells. However, experimental studies are still needed to determine whether the expected improvements in energy alignment, charge transfer, and resistance can be achieved under realistic manufacturing conditions and long-term operating conditions.

5. REAR-INTERFACE PASSIVATION AND INTERLAYER ENGINEERING

Following the development of carbon and graphene-based rear contacts, the next critical design issue is the control of the rear-interface defect chemistry. In this context, interlayer engineering provides a route to simultaneously passivate interfacial traps, regulate energy-level alignment, suppress ion migration, and maintain selective hole extraction in lead-free perovskite solar cells.

5.1. Synergistic Defect Passivation and Chemical Locking at Tin-Perovskite Rear Interfaces

A major challenge limiting both the photovoltaic performance and long-term operational stability of lead-free tin halide perovskite solar cells (TPSCs) is the high density of defects concentrated at grain boundaries and rear interfaces. These defect-rich regions are highly vulnerable to the spontaneous oxidation of Sn^{2+} to Sn^{4+} and the migration of halide ions, particularly I^-. Such processes promote non-radiative charge recombination, local structural and phase degradation, and undesirable self-p-doping, thereby compromising both device efficiency and stability. To simultaneously address these coupled degradation mechanisms, Zhang et al. (2023),[136] introduced a multifunctional “interfacial molecular lock” strategy based on the

(This work is licensed under a Creative Commons Attribution 4.0 International License.)

International Journal of Engineering Research & Technology (IJERT)
ISSN: 2278-0181
Vol. 15 Issue 11 , November - 2026

synergistic incorporation of the pseudohalide anion tetrafluoroborate (BF_4^-) and the polyhydroxylated natural antioxidant myricetin ($C_{15}H_{10}O_8$). From the perspective of lattice structure and interfacial physics, BF_4^- incorporation into the perovskite framework contributes to the relaxation of intrinsic microstrain and enhances the structural stability of the perovskite phase. At the same time, the electron-rich myricetin molecules preferentially interact with the perovskite surface and grain boundaries through strong multidentate hydrogen-bonding interactions. As schematically depicted in Figure X, the resulting molecular network functions as a multifunctional electronic and chemical barrier. The phenolic hydroxyl groups of myricetin provide a localized reducing environment that suppresses the oxidation of Sn^{2+} to Sn^{4+} and can facilitate the reduction of pre-existing oxidized tin sites back to the photoactive Sn^{2+} state. In parallel, the steric and electrostatic interactions within the interfacial network restrict the mobility of iodide ions and help stabilize them within the $[SnI_6]^{4-}$ octahedral framework. These combined effects substantially reduce the density of interfacial trap states (Ntrap), thereby alleviating Fermi-level pinning and promoting longer charge-carrier lifetimes at the rear junction. When applied to the tailored perovskite composition $(MA_{0.25}FA_{0.75})_{0.98}EDA_{0.01}SnI_{2.99}(BF_4)_{0.01}$, this synergistic passivation strategy enabled the resulting devices to reach a power conversion efficiency (PCE) of 14.08%. More importantly, the devices exhibited substantially improved operational durability, retaining 89.9% of their initial efficiency after 200 h of continuous 1-sun illumination and showing negligible degradation following 1,000 h of dark storage (Zhang et al., 2023). These results highlight that effective rear-interface engineering in lead-free tin perovskite photovoltaics requires more than simple energetic-level optimization or external physical encapsulation. Instead, multifunctional interfacial strategies that simultaneously provide chemical reduction, lattice-strain relaxation, and ionic confinement offer a more comprehensive approach to suppressing interfacial recombination and parasitic ion migration. Such synergistic molecular locking strategies therefore represent a promising route toward stabilizing Sn^{2+} chemistry, preserving interfacial electronic quality, and enabling more durable charge extraction in tin-based perovskite solar cells, as shown in figure (9).

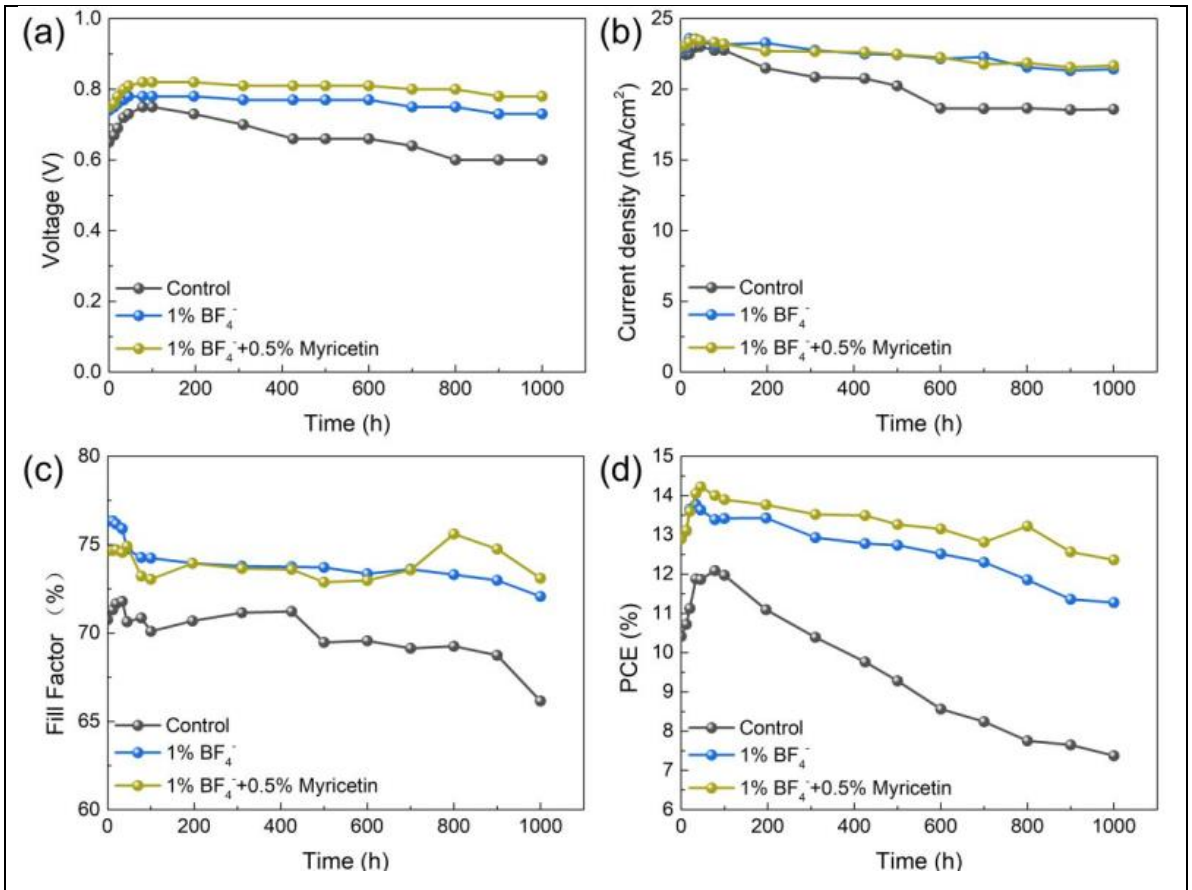


Figure (9): Time-dependent degradation of the photovoltaic performance parameters of molecular-lock-passivated $(MA_{0.25}FA_{0.75})_{0.98}EDA_{0.01}SnI_{2.99}(BF_4)_{0.01}$ tin perovskite solar cells (TPSCs): (a) open-

(This work is licensed under a Creative Commons Attribution 4.0 International License.)

International Journal of Engineering Research & Technology (IJERT)
ISSN: 2278-0181
Vol. 15 Issue 11 , November - 2026

circuit voltage (VOC); (b) short-circuit current density (JSC); (c) fill factor (FF); and (d) power conversion efficiency (PCE)[136]

This figure provides direct evidence supporting the fifth axis, back-end passivation and interlayer engineering, by demonstrating the effectiveness of a dual passivation strategy based on BF_4^- and myricetin ions. The synergistic effect of these two components inhibits the oxidation of Sn^{2+} ions to Sn^{4+}, while simultaneously inhibiting the migration of harmful iodide ions at grain boundaries and back-ends. By effectively reducing interfacial defects and suppressing non-radiative recombination pathways, the molecular passivation strategy mitigates interface and phase degradation, thus preserving the characteristics of the photovoltaic cells during prolonged operation. In particular, the passivated cells maintain relative stability in open-circuit voltage (V_{OC}) and fill factor (F_F), and retain a standard power conversion efficiency (PCE) exceeding 12% after 1000 hours of continuous operation, in stark contrast to the rapid performance degradation observed in the non-passivated controller. These results highlight the crucial role of synergistic molecular passivation in stabilizing the back interface and maintaining efficient and sustainable charge extraction in tin-based perovskite solar cells. Beyond molecular additives and small-molecule chelating agents, the integration of functionalized two-dimensional (2D) carbon networks has emerged as an effective interfacial engineering strategy for suppressing non-radiative recombination and mitigating field-driven ion migration. In perovskite solar cells, ion redistribution and localized halide segregation at grain boundaries and rear charge-selective interfaces can significantly accelerate phase instability and promote the formation of deep-level defect states. Addressing these degradation pathways, Li et al. (2020) developed solution-processable, ultrathin 2D oxo-functionalized graphene nanosheets modified with dodecylamine (oxo-G/DA) and incorporated them into triple-cation $Cs_{0.05}(FA_{0.85}MA_{0.15})_{0.95}Pb(I_{0.85}Br_{0.15})_3$ perovskite solar cells. Firure(10), From a mechanistic perspective, the oxo-G/DA nanosheets perform complementary chemical and electronic functions at both internal grain boundaries and rear interfaces. Oxygen-containing C–O functionalities, together with the delocalized π-conjugated carbon framework, provide electron-rich sites capable of interacting strongly with undercoordinated surface cations, thereby reducing the density of electronically active defects. Meanwhile, the dodecylamine chains facilitate uniform nanosheet dispersion and contribute to the passivation of interfacial grain boundaries. The resulting 2D carbonaceous network closely conforms to the perovskite grains, helping to alleviate localized lattice strain, as evidenced by the formation of interfacial Moiré fringes. At the same time, it functions as a physical and electrostatic barrier that restricts the migration of mobile halide ions, including I^- and Br^-, as well as the redistribution of organic cations under an applied electric field.[137]

(This work is licensed under a Creative Commons Attribution 4.0 International License.)

International Journal of Engineering Research & Technology (IJERT)
ISSN: 2278-0181
Vol. 15 Issue 11 , November - 2026

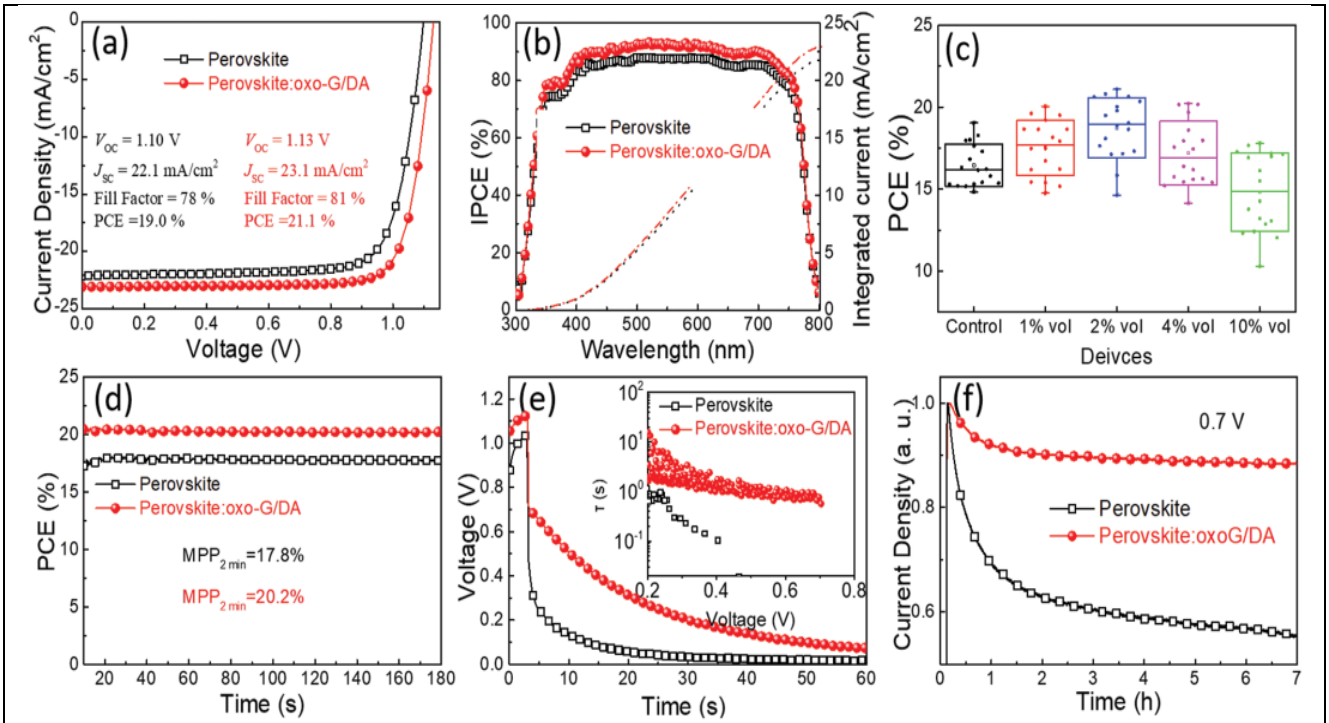


Figure (10): a) J–V curves of the control and doped oxo-G/DA devices under 100 mW cm−2. b) IPCE spectra and c) histogram of PCEs. d) Steady-state efficiency of control and the optimized perovskite-oxo-G/DA solar cells at the maximum power point. e) Open-circuit photovoltage decay (OCVD) curves for the two devices. The inset is the calculated carrier lifetime curve. f) Current transient decay curves for the two devices [137]

The figure demonstrates the impact of incorporating two-dimensional oxo-G/DA nanosheets on optimizing the interfaces within perovskite solar cells. These nanosheets effectively wrap around perovskite grains and their boundaries, while coordinating with under-coordinated defect sites via their oxygen functional groups and dopamine alkylamine chains. This dual interaction successfully passivates defect states and suppresses non-radiative recombination pathways. This effect is clearly evidenced in panel (e) by the prolonged charge carrier lifetime, and in panel (f) by the stabilized current output alongside the suppression of cation and halide ion migration. Consequently, this figure directly correlates with Theme 5 (Rear-Interface Passivation and Interlayer Engineering), illustrating how an ultrathin carbon-based interlayer can simultaneously achieve defect passivation, charge transport regulation, and ion migration inhibition. This interfacial enhancement translates into an elevated power conversion efficiency (PCE) of 21.1%, an enhanced fill factor (*FF*) of 81%, and an exceptional operational stability—retaining approximately 70% of its initial efficiency after 960 hours of unencapsulated storage. Overall, these results demonstrate that rationally designed 2D functionalized carbon interlayers can simultaneously address electronic and ionic losses at perovskite interfaces. By chemically anchoring undercoordinated species, passivating interfacial defects, relaxing localized structural strain, and restricting the migration of volatile ions, such carbonaceous networks provide a powerful route for minimizing rear-contact recombination and suppressing long-term phase degradation. Their multifunctional nature therefore makes 2D interlayer engineering a promising strategy for achieving efficient and durable perovskite photovoltaic devices.[137].

Wang et al.[138] investigated the interfacial modification of lead-free $Cs_2AgBiBr_6$ mesoporous TiO_2-based perovskite solar cells by sensitizing the mesoporous TiO_2 electron-transport layer with a carboxylated chlorophyll derivative (C-Chl). The C-Chl molecules were introduced prior to the deposition of the perovskite absorber, indicating that the modification primarily targets the front $TiO_2/Cs_2AgBiBr_6$ electron-extraction interface rather than the rear hole-transport or back-contact interface. Nevertheless, the study provides relevant evidence for the broader interfacial-engineering aspects of Theme 5. The incorporation of C-Chl resulted in a substantial reduction in charge-transfer resistance, from 1731.0 Ω for the pristine device to 318.5 Ω for the modified device. In addition, the photoluminescence decay lifetime decreased from 8.13

(This work is licensed under a Creative Commons Attribution 4.0 International License.)

International Journal of Engineering Research & Technology (IJERT)
ISSN: 2278-0181
Vol. 15 Issue 11 , November - 2026

to 3.54 ns, suggesting more efficient charge extraction and reduced charge accumulation at the modified interface. These interfacial improvements translated into enhanced photovoltaic performance, with the average power conversion efficiency (PCE) increasing from 2.06% to 2.94%. This improvement was accompanied by an increase in the short-circuit current density ((Jsc)) from 3.13 to 3.98 mA cm^{-2} under reverse scanning. As shown in figure(22)

Although this study does not directly demonstrate passivation of the rear interface, it highlights molecular interlayers can effectively regulate interfacial charge transfer and mitigate recombination losses when their chemical functionalities and electronic structures are appropriately matched with those of the adjacent semiconductor. Therefore, the C-Chl/TiO_2 approach can be considered complementary evidence supporting the role of molecular interlayer engineering in improving interfacial charge dynamics, while its direct relevance to rear-interface passivation remains limited.

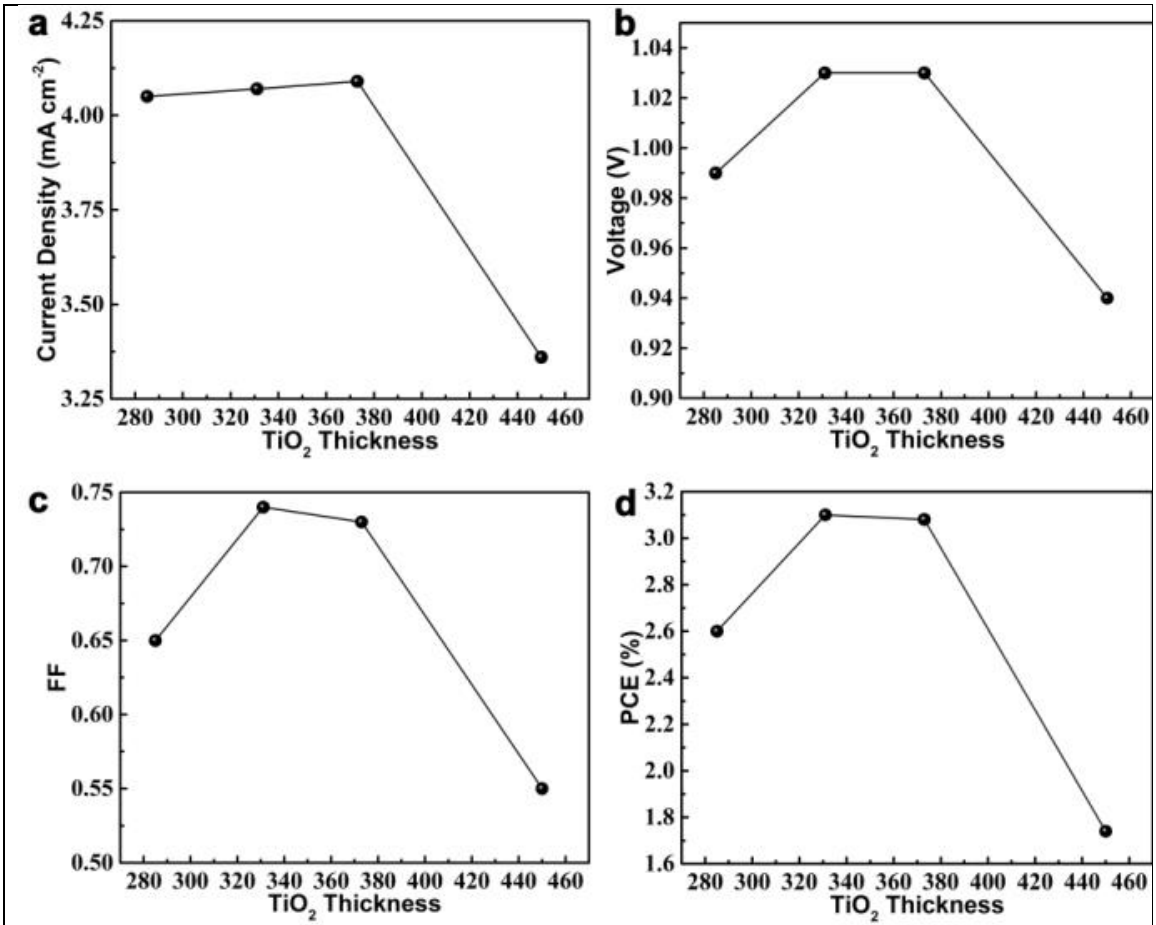


Figure (11): Solar cell performance parameters as a function of TiO2 thickness for Cs2AgBiBr6-based PSCs with CChl. (a) Short-circuit current density, (b) open-circuit voltage, (c) fill factor, and (d) power conversion efficiency[138]

A key structural parameter in front-interface engineering is the precise control of the mesoporous electron-transport scaffold thickness. The systematic optimization of carboxylated chlorophyll-sensitized mesoporous TiO_2 (m-TiO_2/C-Chl) for $Cs_2AgBiBr_6$ solar cells, as presented in Figure S3, demonstrates that photovoltaic performance is strongly influenced by a fundamental balance between charge transport and interfacial accessibility. An optimal m-TiO_2 thickness in the range of 330–375 nm provides sufficient surface area for enhanced C-Chl loading and improved interfacial contact while avoiding excessive series resistance (R_s). Under these conditions, the devices achieve a maximum power conversion efficiency (PCE) of approximately 3.1%, together with an enhanced short-circuit current density (J_sc) exceeding 4.0 mA cm^{-2} and an open-circuit voltage (Voc) of 1.03 V.

(This work is licensed under a Creative Commons Attribution 4.0 International License.)

International Journal of Engineering Research & Technology (IJERT)
ISSN: 2278-0181
Vol. 15 Issue 11 , November - 2026

5.2. Back-Contact Engineering in Different Lead-Free Absorber Families

Although front-contact engineering and internal defect passivation are essential for improving the performance of lead-free perovskite solar cells, the back-contact structure remains a critical constraint that ultimately determines charge carrier extraction, interfacial recombination, chemical stability, and long-term operational durability. Unlike conventional lead halide perovskites, lead-free absorbers exhibit entirely different electronic structures, defect chemical compositions, and degradation pathways. Therefore, a single back-contact strategy cannot be universally applied to a wide range of lead-free perovskite formulations.

5.2.1. Tin Perovskites:

Tin perovskites are particularly susceptible to the rapid and spontaneous oxidation of tin(II) ions (Sn^{2+}) to tin(IV) ions (Sn^{4+}), as well as the cross-dilution of halide and metal ions at the back-facial interface. These challenges necessitate the development of hole-transporting layers (HTLs) with compatible valence band energy levels ($E_v \approx -5.2$ to -5.5 eV), high chemical compatibility with metal electrodes, and effective resistance to electrode-induced degradation, including gold and silver migration. The incorporation of hydrophobic, self-encapsulating interfacial barriers can limit moisture intrusion and mitigate chemical degradation at the back surface.

5.2.2. Double perovskites ($A_2M'M''X_6$, such as $Cs_2AgBiBr_6$):

Double perovskites generally exhibit large energy gaps ($E^g > 2.0$ eV) and relatively deep valence band sites ($E_v < -6.0$ eV), resulting in significant energy contrasts with conventional organic hole-transporting layers such as Spiro-OMeTAD and PTAA. Energy band mismatch can lead to significant extraction barriers at the interface, thus limiting the open-circuit potential (V_oc). To overcome these limitations, inorganic interlayers with deep work functions, including NiO_x, CuSCN, CuI, and polyaxials, along with appropriately engineered carbon back electrodes, offer promising pathways for improving energy compatibility and reducing losses at the interface.

Bismuth and antimony halides and chalcogenides ($A_3M_2X_9$/$MA_3Bi_2I_9$): Bismuth and antimony-based adsorbents are characterized by highly anisotropic charge carrier transport and pronounced chemical interactions at the interfaces. Therefore, their back contact surfaces require structure-specific engineering strategies capable of passivating exposed metal sites with low coordination, while simultaneously suppressing ion migration and interactions at the interface under the influence of electrical bias. Effective control of these processes is essential to minimize non-radiative recombination and maintain device stability during prolonged operation[139].

5.2.3. Carbon and hole-transfer-free architectures:

Carbon electrodes and hole-transfer-free device configurations offer an attractive alternative to conventional precious metal connectors due to their lower cost, scalability, ease of printing, and relatively high chemical and environmental stability. However, their application introduces additional challenges, particularly in minimizing series resistance and achieving optimal energy compatibility between surfaces. Therefore, the successful integration of carbon electrodes requires simultaneous optimization of electrode conductivity, contact selectivity, interfacial passivation, and energy level matching with the lead-free perovskite layer. Generally, the back contact surface should be viewed not merely as a passive electrode element, but as an active functional layer. Its electronic structure, chemical compatibility, and chemical defect composition must be designed to match the lead-free perovskite structure. The contact geometry of the assembly is essential to maximizing charge carrier extraction, inhibiting interfacial recombination, reducing ion migration and chemical degradation, and ultimately extending the operational life of low-phase solar cells. In tin-based perovskite solar cells (TPSCs), the back-contact architecture performs a critical dual function by providing an energetically favorable pathway for efficient hole extraction while simultaneously acting as a protective barrier against environmental degradation, particularly oxygen and moisture ingress, as well as halide–metal interdiffusion. As comprehensively reviewed by Ayaydah et al.[139], the development of chemically stable and electrically efficient rear interfaces in ASnX3 perovskites is strongly governed by the selection of both the hole transport layer (HTL) and the counter-electrode material. Conventional hole-selective materials such as spiro-OMeTAD present significant limitations in tin-based systems because their operation typically relies on hygroscopic oxidative dopants, including Li-TFSI and 4-tert-butylpyridine (tBP). These dopants can promote excessive p-type doping and accelerate the undesirable oxidation of Sn2+ to Sn4+, thereby

(This work is licensed under a Creative Commons Attribution 4.0 International License.)

International Journal of Engineering Research & Technology (IJERT)
ISSN: 2278-0181
Vol. 15 Issue 11 , November - 2026

increasing defect formation and compromising the chemical stability of the perovskite absorber. Moreover, their presence can facilitate metal-ion migration from metallic electrodes, particularly Ag and Au, into the perovskite layer, resulting in additional interfacial degradation. Likewise, PEDOT:PSS, which is widely employed in inverted (p-i-n) device architectures, suffers from intrinsic acidity and hygroscopicity. These properties can promote interfacial chemical reactions, electrode corrosion, and the formation or accumulation of non-radiative trap states, ultimately limiting both device efficiency and operational stability. To mitigate these degradation pathways, recent contact-engineering approaches have increasingly focused on dopant-free and chemically robust inorganic HTLs. In particular, p-type inorganic semiconductors such as NiOx and CuSCN offer enhanced chemical stability, suitable work functions, and favorable valence-band alignment with tin-based perovskite absorbers. Their valence-band energy levels, typically within the range of EV = -5.3 to -5.5 eV, provide an energetically compatible interface with the relatively shallow valence-band maximum of FASnI3 (Figure 12), thereby facilitating efficient hole extraction while minimizing energetic barriers. Notably, optimized CuSCN-based rear-contact structures have achieved power-conversion efficiencies exceeding 7.3%, while simultaneously avoiding the interfacial shunting and degradation associated with conventional molecular dopants.[139].

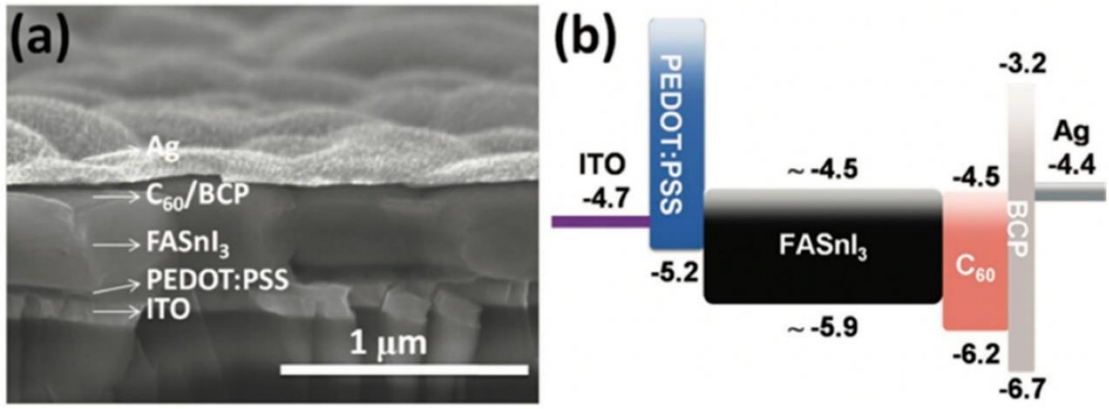


Figure (12): (a) SEM image of an inverted FASnI3 perovskite solar cell with SnF2 additive at 10 mol%. (b) System energy level diagram of FASnI3. Reproduced with permission.[139].

An alternative strategy involves eliminating the organic HTL altogether through HTL-free device architectures combined with carbon-based back electrodes. This configuration can substantially reduce the possibility of undesirable halide–metal reactions and offers additional advantages in terms of material cost, chemical robustness, and manufacturing simplicity. Nevertheless, the absence of a dedicated hole-selective interlayer places greater emphasis on controlling the electrode work function and the perovskite/electrode interface. Precise work-function engineering is therefore essential to minimize energy-level mismatches, suppress interfacial charge accumulation, and maintain efficient carrier extraction. Collectively, these developments highlight the importance of composition-specific back-contact engineering as a key strategy for simultaneously improving the efficiency, chemical stability, and long-term operational durability of TPSCs.

REFERENCES

[1] REN21, *Renewables 2023 Global Status Report*, REN21 Secretariat, Paris, 2023.
[2] International Energy Agency (IEA), *World Energy Outlook 2023*, IEA, Paris, 2023.
[3] IPCC, *Climate Change 2023: Synthesis Report*, Intergovernmental Panel on Climate Change, Geneva, 2023.
[4] M.A. Green, E.D. Dunlop, J. Hohl-Ebinger, M. Yoshita, N. Kopidakis, X. Hao, Solar cell efficiency tables (version 64), *Prog. Photovolt. Res. Appl.* 32 (2024) 3–13.
[5] A. Richter, M. Hermle, S.W. Glunz, Reassessment of the limiting efficiency for crystalline silicon solar cells, *IEEE J. Photovolt.* 3 (2013) 1184–1191.
[6] M.A. Green, Third generation photovoltaics: solar cells for 2020 and beyond, *Physica E* 14 (2002) 65–70.
[7] A. Kojima, K. Teshima, Y. Shirai, T. Miyasaka, Organometal halide perovskites as visible-light sensitizers for photovoltaic cells, *J. Am. Chem. Soc.* 131 (2009) 6050–6051.
[8] M.M. Lee, J. Teuscher, T. Miyasaka, T.N. Murakami, H.J. Snaith, Efficient hybrid solar cells based on meso-superstructured organometal halide perovskites, *Science* 338 (2012) 643–647.
[9] National Renewable Energy Laboratory (NREL), *Best Research-Cell Efficiency Chart*, Golden, CO, updated 2024.

(This work is licensed under a Creative Commons Attribution 4.0 International License.)

International Journal of Engineering Research & Technology (IJERT)
ISSN: 2278-0181
Vol. 15 Issue 11 , November - 2026

[10] M.A. Green, A. Ho-Baillie, H.J. Snaith, The emergence of perovskite solar cells, *Nat. Photonics* 8 (2014) 506–514.
[11] F.P.G. de Arquer, A. Armin, P. Meredith, E.H. Sargent, Solution-processed semiconductors for next-generation photodetectors and solar cells, *Nat. Rev. Mater.* 2 (2017) 16100.
[12] H. Min, D.Y. Lee, J. Kim, et al., Perovskite solar cells with atomically coherent interlayers on SnO2_22 electrodes, *Nature* 598 (2021) 444–450
[13] M. Saliba, T. Matsui, J.Y. Seo, et al., Cesium-containing triple cation perovskite solar cells: improved stability, reproducibility and high efficiency, *Energy Environ. Sci.* 9 (2016) 1989–1997.
[14] H. Tsai, W. Nie, J.C. Blancon, et al., High-efficiency two-dimensional Ruddlesden–Popper perovskite solar cells, *Nature* 536 (2016) 312–316.
[15] S.D. Stranks, H.J. Snaith, Metal-halide perovskites for photovoltaic and light-emitting devices, *Nat. Nanotechnol.* 10 (2015) 391–402.
[16] G. Grancini, M.K. Nazeeruddin, Dimensional tailoring of hybrid perovskites for photovoltaics, *Nat. Rev. Mater.* 4 (2019) 4–22
[17] D.B. Mitzi, K. Chondroudis, C.R. Kagan, Design, structure, and optical properties of organic–inorganic perovskites containing tin and lead halides, *Inorg. Chem.* 38 (1999) 6246–6256.
[18] G.E. Eperon, S.D. Stranks, C. Menelaou, et al., Formamidinium lead trihalide: a broadly tunable perovskite for efficient planar heterojunction solar cells, *Energy Environ. Sci.* 7 (2014) 982–988.
[19] W.-J. Yin, T. Shi, Y. Yan, Unusual defect physics in CH3_33NH3_33PbI3_33 perovskite solar cell absorber, *Appl. Phys. Lett.* 104 (2014) 063903.
[20] A.M. Ganose, C.N. Savory, D.O. Scanlon, Beyond methylammonium lead iodide: prospects for the emergent field of ns2^22-containing solar absorbers, *Chem. Commun.* 53 (2017) 20–44.
[21] M.G. Kanatzidis, Halide perovskites: poor man's high-performance semiconductors, *Nat. Mater.* 16 (2017) 899–900.
[22] J.-P. Correa-Baena, M. Saliba, T. Buonassisi, et al., Promises and challenges of perovskite solar cells, *Science* 358 (2017) 739–744.
[23] W.S. Yang, B.-W. Park, E.H. Jung, et al., Iodide management in formamidinium-lead-halide–based perovskite layers for efficient solar cells, *Science* 356 (2017) 1376–1379.
[24] T. Leijtens, G.E. Eperon, N.K. Noel, S.N. Habisreutinger, A. Petrozza, H.J. Snaith, Stability of metal halide perovskite solar cells, *Adv. Energy Mater.* 5 (2015) 1500963.
[25] J.A. Christians, P.A. Miranda Herrera, P.V. Kamat, Transformation of the excited state and photovoltaic efficiency of CH3_33 NH3_33PbI3_33 perovskite upon controlled exposure to humidified air, *J. Am. Chem. Soc.* 137 (2015) 1530–1538.
[26] N.-G. Park, Perovskite solar cells: an emerging photovoltaic technology, *Mater. Today* 18 (2015) 65–72.
[27] Y. Rong, L. Liu, A. Mei, X. Li, H. Han, Beyond efficiency: the challenge of stability in mesoscopic perovskite solar cells, *Adv. Energy Mater.* 5 (2015) 1501066.
[28] B. Zhao, S. Bai, V. Kim, et al., High-efficiency perovskite–polymer bulk heterostructure light-emitting diodes, *Nat. Photonics* 12 (2018) 783–789.
[29] R.E. Brandt, V. Stevanović, D.S. Ginley, T. Buonassisi, Identifying defect-tolerant semiconductors with high minority-carrier lifetimes: beyond hybrid lead halide perovskites, *MRS Commun.* 5 (2015) 265–275.
[30] T.M. Koh, T. Krishnamoorthy, N. Yantara, et al., Formamidinium tin-based perovskite with low Eg for photovoltaic applications, *J. Mater. Chem. A* 3 (2015) 14996–15000.
[31] T. Krishnamoorthy, H. Ding, C. Yan, et al., Lead-free germanium iodide perovskite materials for photovoltaic applications, *J. Mater. Chem. A* 3 (2015) 23829–23832.
[32] F. Hao, C.C. Stoumpos, D.H. Cao, R.P.H. Chang, M.G. Kanatzidis, Lead-free solid-state organic–inorganic halide perovskite solar cells, *Nat. Photonics* 8 (2014) 489–494.
[33] F. Hao, C.C. Stoumpos, R.P.H. Chang, M.G. Kanatzidis, Anomalous band gap behavior in mixed Sn and Pb perovskites enables broadening of absorption spectrum in solar cells, *J. Am. Chem. Soc.* 136 (2014) 8094–8099.
[34] W. Ke, C.C. Stoumpos, M.G. Kanatzidis, "Unleaded" perovskites: status quo and future prospects of tin-based perovskite solar cells, *Adv. Mater.* 31 (2019) 1803230.
[35] T. Bin Song, T. Yokoyama, S. Aramaki, M.G. Kanatzidis, Performance enhancement of lead-free tin-based perovskite solar cells with reducing atmosphere-assisted dispersible additive, *ACS Energy Lett.* 2 (2017) 897–903.
[36] A. Abate, Perovskite solar cells go lead free, *Joule* 1 (2017) 659–664.
[37] W. Ke, M.G. Kanatzidis, Prospects for low-toxicity lead-free perovskite solar cells, *Nat. Commun.* 10 (2019) 965.
[38] C.C. Stoumpos, C.D. Malliakas, M.G. Kanatzidis, Semiconducting tin and lead iodide perovskites with organic cations: phase transitions, high mobilities, and near-infrared photoluminescent properties, *Inorg. Chem.* 52 (2013) 9019–9038.
[39] Y. Shao, Y. Yuan, J. Huang, Correlation of energy disorder and open-circuit voltage in hybrid perovskite solar cells, *Nat. Energy* 1 (2016) 15001.
[40] N.K. Noel, S.D. Stranks, A. Abate, et al., Lead-free organic–inorganic tin halide perovskites for photovoltaic applications, *Energy Environ. Sci.* 7 (2014) 3061–3068.
[41] I. Chung, B. Lee, J. He, R.P.H. Chang, M.G. Kanatzidis, All-solid-state dye-sensitized solar cells with high efficiency using perovskite absorbers, *Nature* 485 (2012) 486–489.
[42] A. Marshall, R.E. Brandt, D.H. Cao, et al., Cesium tin halide perovskites for photovoltaics: composition and phase engineering, *J. Phys. Chem. Lett.* 11 (2020) 620–627.
[43] B. Pospischil, M.M. Tavakoli, H. Han, Stability issues in tin halide perovskites, *Adv. Funct. Mater.* 31 (2021) 2008185
[44] J. Heo, J.H. Im, Y. Heo, K. Lee, T.K. Ahn, N.-G. Park, Efficient inorganic–organic hybrid heterojunction solar cells containing perovskite compound and polymeric hole conductors, *Nat. Photonics* 7 (2013) 486–491
[45] H.J. Park, SCAPS-1D simulation for device optimization to improve efficiency in lead-free CsSnI3_33 perovskite solar cells, *Inorganics* 12 (2024) 123.

(This work is licensed under a Creative Commons Attribution 4.0 International License.)

International Journal of Engineering Research & Technology (IJERT)
ISSN: 2278-0181
Vol. 15 Issue 11 , November - 2026

[46] E. Danladi, S.A. Alatawi, A.A. Alharthi, et al., 20.730% highly efficient lead-free CsSnI3_33-based perovskite solar cells with various charge transport materials: a SCAPS-1D study, *Multiscale Multidiscip. Model. Exp. Des.* 8 (2024) 114

[47] A Comprehensive Study of CsSnI3_33-Based Perovskite Solar Cells with Efficient Charge Transport Materials and Various Metal Back Contacts, *Micromachines* 14 (2023) 1562.

[48] T.M. Koh, T. Krishnamoorthy, N. Yantara, et al., Formamidinium tin-based perovskite with low Eg for photovoltaic applications, *J. Mater. Chem. A* 3 (2015) 14996–15000.

[49] L. Ran, W. Ke, C.C. Stoumpos, M.G. Kanatzidis, Tin halide perovskite solar cells in the spotlight: stability and efficiency, *Adv. Energy Mater.* 10 (2020) 1903191.

[50] C. Liu, W. Li, C. Zhang, et al., Efficient lead-free FASnI3_33 perovskite solar cells enabled by interface engineering, *J. Mater. Chem. A* 8 (2020) 10337–10345

[51] Y. Wang, T. Zhang, M. Kan, Y. Zhao, Bifunctional stabilization of all-inorganic α-CsPbI3_33 perovskite for 17% efficiency photovoltaics, *J. Am. Chem. Soc.* 140 (2018) 12345–12348.

[52] A. Mei, X. Li, L. Liu, et al., A hole-conductor–free, fully printable mesoscopic perovskite solar cell with high stability, *Science* 345 (2014) 295–298.

[53] F. Di Giacomo, H. Razza, F. Matteocci, et al., High efficiency and stable perovskite solar cells with low-temperature carbon-based electrodes, *Adv. Energy Mater.* 5 (2015) 1401808.

[54] X. Zhang, M. Liu, W. Eperon, et al., Carbon-based materials for perovskite solar cells, *Adv. Energy Mater.* 8 (2018) 1702498.

[55] N. Kumar, M. Chandra, M. Muddassir, Progress in MASnI3_33-based lead-free perovskite solar cells, *Sol. Energy Mater. Sol. Cells* 230 (2021) 111216.

[56] D. Sabba, H.K. Mulmudi, R.R. Prabhakar, et al., Impact of anionic Br substitution on open circuit voltage in lead free perovskite (CsSnI3_33) solar cells, *J. Phys. Chem. C* 119 (2015) 1763–1767.

[57] W. Ke, C.C. Stoumpos, J.L. Logsdon, et al., Enhancing lead-free tin halide perovskite solar cell performance through oxidation suppression, *J. Am. Chem. Soc.* 138 (2016) 14998–15003

[58] N. Noel, A. Abate, S.D. Stranks, et al., Enhanced performance in tin halide perovskite solar cells by controlled interfaces and contacts, *ACS Nano* 8 (2014) 9815–9821.

[59] M. Jørgensen, K. Norrman, F.C. Krebs, Stability/degradation of polymer solar cells, *Sol. Energy Mater. Sol. Cells* 92 (2008) 686–714.

[60] D. Sabba, H.K. Mulmudi, R.R. Prabhakar, et al., Mixed-halide tin perovskites for lead-free photovoltaics, *J. Phys. Chem. C* 119 (2015) 1763–1767.

[61] Y. Ogomi, A. Morita, S. Tsukamoto, et al., CH3_33NH3_33Snx_xxPb1−x_{1-x}1−xI3_33 perovskite solar cells covering up to 1060 nm, *J. Phys. Chem. Lett.* 5 (2014) 1004–1011.

[62] G.E. Eperon, V.M. Burlakov, P. Docampo, et al., Morphological control for high performance, solution-processed planar heterojunction perovskite solar cells, *Adv. Funct. Mater.* 24 (2014) 151–157.

[63] H.J. Park, Band alignment and bromide-content effects in mixed-halide lead-free perovskite absorbers, *J. Mater. Sci. Mater. Electron.* 35 (2024) 1–14

[64] H.J. Snaith, Present status and future prospects of perovskite photovoltaics, *Nat. Mater.* 17 (2018) 372–376.

[65] E.T. Hoke, D.J. Slotcavage, E.R. Dohner, et al., Reversible photo-induced trap formation in mixed-halide hybrid perovskites for photovoltaics, *Chem. Sci.* 6 (2015) 613–617.

[66] A.H. Slavney, T. Hu, A.M. Lindenberg, H.I. Karunadasa, A bismuth-halide double perovskite with long carrier recombination lifetime for photovoltaic applications, *J. Am. Chem. Soc.* 138 (2016) 2138–2141.

[67] E.T. McClure, M.R. Ball, W. Windl, P.M. Woodward, Cs2_22AgBiX6_66 (X = Br, Cl): new visible light absorbing, lead-free halide perovskite semiconductors, *Chem. Mater.* 28 (2016) 1348–1354.

[68] F. Giustino, H.J. Snaith, Toward lead-free perovskite solar cells, *ACS Energy Lett.* 1 (2016) 1233–1240

[69] A.H. Slavney, L. Leppert, D.O. Scanlon, H.I. Karunadasa, Defect-induced band-edge reconstruction of a bismuth-halide double perovskite for visible-light absorption, *J. Am. Chem. Soc.* 139 (2017) 5015–5018.

[70] A. Hossain, S. Kiran, M.M. Rahman, Recent progress in Cs2_22AgBiBr6_66 double perovskite solar absorbers, *Sol. RRL* 6 (2022) 2100894.

[71] M. Shrivastav, A. Pandey, P. Sharma, Improving Cs2_22AgBiBr6_66-based solar cell performance via transport-layer optimization, *Mater. Today Commun.* 36 (2023) 106761.

[72] S. Ahmad, M. Nazeeruddin, T. Brown, Contact and transport layer engineering in double perovskite photovoltaics, *J. Phys. Chem. Lett.* 11 (2020) 10114–10124.

[73] M. Toki, S. Rahman, M. Shahiduzzaman, Numerical design of inorganic charge-transport layers for Cs2_22AgBiBr6_66 solar cells, *Semicond. Sci. Technol.* 38 (2023) 015005.

[74] S. Hoefler, G. Trimmel, T. Rath, Progress on lead-free metal halide perovskites for photovoltaic applications: a review, *Monatsh. Chem.* 148 (2017) 795–826.

[75] A.M. Ganose, C.N. Savory, D.O. Scanlon, Beyond methylammonium lead iodide: prospects for the emergent field of ns2^22-containing solar absorbers, *Chem. Commun.* 53 (2017) 20–44.

[76] T. Rath, W. Peng, R. Huber, et al., Perovskite-inspired materials for photovoltaics and beyond—from design to devices, *Adv. Energy Mater.* 11 (2021) 2002922.

[77] H.J. Snaith, A. Abate, J.M. Ball, et al., Anomalous hysteresis in perovskite solar cells, *J. Phys. Chem. Lett.* 5 (2014) 1511–1515.

[78] Q. Dong, Y. Fang, Y. Shao, et al., Electron-hole diffusion lengths > 175 μm in solution-grown CH3_33NH3_33PbI3_33 single crystals, *Science* 347 (2015) 967–970.

[79] S.M. Sze, K.K. Ng, *Physics of Semiconductor Devices*, 3rd ed., Wiley, Hoboken, 2007.

[80] P. Würfel, U. Würfel, *Physics of Solar Cells: From Basic Principles to Advanced Concepts*, 3rd ed., Wiley-VCH, Weinheim, 2016.

[81] J. Bisquert, *The Physics of Solar Cells: Perovskites, Organics, and Photovoltaic Fundamentals*, CRC Press, Boca Raton, 2018.

(This work is licensed under a Creative Commons Attribution 4.0 International License.)

International Journal of Engineering Research & Technology (IJERT)
ISSN: 2278-0181
Vol. 15 Issue 11 , November - 2026

[82] J.A. Christians, R.C.M. Fung, P.V. Kamat, An inorganic hole conductor for organo-lead halide perovskite solar cells. Improved hole conductivity with copper iodide, *J. Am. Chem. Soc.* 136 (2014) 758–764.

[83] K. Domanski, J.-P. Correa-Baena, N. Mine, et al., Not all that glitters is gold: metal-migration-induced degradation in perovskite solar cells, *ACS Nano* 10 (2016) 6306–6314.

[84] J.H. Noh, S.H. Im, J.H. Heo, T.N. Mandal, S.I. Seok, Chemical management for colorful, efficient, and stable inorganic–organic hybrid nanostructured solar cells, *Nano Lett.* 13 (2013) 1764–1769.

[85] J.A. Christians, J.S. Manser, P.V. Kamat, Best practices in perovskite solar cell efficiency measurements. Avoiding the error of making bad cells look good, *J. Phys. Chem. Lett.* 6 (2015) 852–857.

[86] M. Abdi-Jalebi, Z. Andaji-Garmaroudi, S.D. Stranks, et al., Maximizing and stabilizing luminescence from halide perovskites with potassium passivation, *Nature* 555 (2018) 497–501.

[87] H.J. Park, Work-function dependent back-contact engineering in lead-free perovskite solar cells, *Appl. Opt.* 64 (2025) 4818–4828.

[88] A. Fakharuddin, L. Schmidt-Mende, G. Garcia-Belmonte, R. Jose, I. Mora-Seró, Interfaces in perovskite solar cells, *Adv. Energy Mater.* 7 (2017) 1700623.

[89] D. Crespo-Quesada, T. Miyasaka, Carbon and graphene-derived electrodes in perovskite solar cells, *ChemSusChem* 12 (2019) 4512–4528.

[90] M. Burgelman, P. Nollet, S. Degrave, Modelling polycrystalline semiconductor solar cells, *Thin Solid Films* 361–362 (2000) 527–532.

[91] M. Burgelman, K. Decock, A. Niemegeers, J. Verschraegen, S. Degrave, SCAPS manual and application examples, University of Gent, Belgium, 2019.

[92] V.H.D. Araújo, A.F. Nogueira, J.C. Tristão, L.J.D. Santos, Advances in lead-free perovskite solar cell design via SCAPS-1D simulations, *RSC Sustainability* 3 (2025) 4314–4335.

[93] Simon M. Sze, Kwok K. Ng , Physics of Semiconductor Devices, 3rd Edition, ISBN: 978-0-470-06832-8, April 2006, 832 pages, https://www.wiley.com/en-us/shop/general-introductory-electrical-electronics-engineering/physics-of-semiconductor-devices-3rd-edition-p-9780470068328.

[94] Talal H. Alzanki, Kandil M. Kandil, Adapting Integrated High Concentrated PV Modules and Evacuated Tube Collectors to Minimize Building Energy Consumption in Hot Climate, Smart Grid and Renewable Energy, Vol.10 No.10, October 23, 2019, https://www.scirp.org/reference/referencespapers?referenceid=2640362.

[95] Samia Sayed Mustafa Shaban, The Solar Cell Parameters as a Function of Its Temperature in Relation to Its Diurnal Efficiency, Optics and Photonics Journal, Vol.10 No.1, February 20, 2020, https://www.scirp.org/reference/referencespapers?referenceid=2683227.

[96] L. J. Chen, C. R. Lee, Y. J. Chuang, Z. H. Wu, and C. Chen,"Synthesis and Optical Properties of Lead-Free Cesium Tin Halide Perovskite Quantum Rods with High-Performance Solar Cell Application," Journal of Physical Chemistry Letters, vol. 7, no. 24, pp. 5028–5035, Dec. 2016, doi: 10.1021/acs.jpclett.6b02344.

[97] A. Rajagopal, K. Yao, and A. K. Y. Jen, "Toward Perovskite Solar Cell Commercialization: A Perspective and Research Roadmap Based on Interfacial Engineering," *Advanced Materials*, vol. 30, no. 32, Art. no. 1800455, 2018. https://doi.org/10.1002/adma.201800455.

[98] W. S. Yang, J. H. Noh, N. J. Jeon, Y. C. Kim, S. Ryu, J. Seo, and S. I. Seok, "Iodide Management in Formamidinium-Lead-Halide-Based Perovskite Layers for Efficient Solar Cells," *Science*, vol. 356, no. 6345, pp. 1376–1379

[99] Ossila, "Spiro-OMeTAD (Spiro-MeOTAD) | >99.0% | 207739-72-8," *Ossila Product Database*. [Online]. Available: https://www.ossila.com/products/spiro-ometad.

[100] Mohammad Sharabi, Muwaffaq Raqia, Saeed Mandou, Improving the Performance of Lead-Free Perovskite Solar Cells Using Cost-Effective Gold Substitutes via Numerical Simulation, Idlib University Journal of Research, Volume 9, Issue 1, 2026..

[101] Das, A.; Peu, S.D.; Akanda, M.A.M.; Salah, M.M.; Hossain, M.S.; Das, B.K. Numerical Simulation and Optimization of Inorganic Lead-Free Cs3Bi2I9-Based Perovskite Photovoltaic Cell: Impact of Various Design Parameters. Energies 2023, 16, 2328. https://doi.org/10.3390/en16052328.

[102] R. Tala-Ighil Zaïr, C. Oudjehani, and K. Tighilt, "SCAPS Simulation for Perovskite Solar Cell," *Journal of Solar Energy Research Updates*, vol. 8, pp. 21–26, Oct. 2025. doi: 10.31875/2410-2199.2021.08.3.

[103] O. A. Muhammed, D. Eli, P. H. Boduku, J. Tasiu, M. S. Ahmad, and N. Usman, "Modeling and simulation of lead-free perovskite solar cell using SCAPS-1D," *East European Journal of Physics*, vol. 2021, no. 2, pp. 146–154, 2021. doi: 10.26565/2312-4334-2021-2-12.

[104] K. D. Jayan and V. Sebastian, "Comprehensive device modelling and performance analysis of MASnI3 based perovskite solar cells with diverse ETM, HTM and back metal contacts," *Solar Energy*, vol. 217, pp. 40–48, Mar. 2021. doi: 10.1016/j.solener.2021.01.058.

[105] M. K. Hossain *et al.*, "Deep Insights into the Coupled Optoelectronic and Photovoltaic Analysis of Lead-Free CsSnI3 Perovskite-Based Solar Cell Using DFT Calculations and SCAPS-1D Simulations," *ACS Omega*, vol. 8, no. 25, pp. 22466–22485, Jun. 2023. doi: 10.1021/acsomega.3c00306.

[106] Seyed-Talebi SM, Mahmoudi M, Lee CH. A Comprehensive Study of $CsSnI_3$-Based Perovskite Solar Cells with Different Hole Transporting Layers and Back Contacts. Micromachines (Basel). 2023 Aug 6;14(8):1562. PMID: 37630098; PMCID: PMC10456552. doi: 10.3390/mi14081562.

[107] Shockley, W.; Read, W. T. Statistics of the recombinations of holes and electrons. Phys. Rev. 1952, 87, 835–842.

[108] Noel, N. K.; Stranks, S.D.; Abate, A.; Wehrenfennig, C.; Guarnera, S.; Haghighirad, A.-A.; Sadhanala, A.; Eperon, G.E.; Pathak, S. K.; Johnston, M.B.; Petrozza, A.; Herz, L.M.; Snaith, H. J. Lead-Free Organic–Inorganic Tin Halide Perovskites for Photovoltaic Applications. Energy Environ. Sci. 2014, 7, 3061–3068

[109] Koh, T.M.; Krishnamoorthy, T.; Yantara, N.; Shi, C.; Leong, W.L.; Boix, P.P.; Grätzel, M.; Mathews, N.; Mhaisalkar, S. G. Formamidinium Tin-Based Perovskite with Low Eg for Photovoltaic Applications. J. Mater. Chem. A 2015, 3, 14996–15000.

(This work is licensed under a Creative Commons Attribution 4.0 International License.)

[110] Ke, W.; Stoumpos, C.C.; Kanatzidis, M. G. "Unleaded" Perovskites: Status Quo and Future Prospects of Tin-Based Perovskite Solar Cells. Adv. Mater. 2019, 31, 1803230

[111] Slavney, A.H.; Hu, T.; Lindenberg, A.M.; Karunadasa, H. I. A Bismuth-Halide Double Perovskite with Long Carrier Recombination Lifetime for Photovoltaic Applications. J.Am. Chem. Soc. 2016, 138, 2138–2141.

[112] Huang, Y.; Kavanagh, S. R.; Scanlon, D. O.; Walsh, A.; Hoye, R. L. Z. Perovskite-inspired materials for photovoltaics and beyond—from design to devices. Nanotechnology 2021, 32, 132004.

[113] Seyed-Talebi SM, Mahmoudi M, Lee CH. A Comprehensive Study of $CsSnI_3$-Based Perovskite Solar Cells with Different Hole Transporting Layers and Back Contacts. Micromachines (Basel). 2023 Aug 6;14(8):1562. PMID: 37630098; PMCID: PMC10456552. doi: 10.3390/mi14081562.

[114] N. Sultana, O. Islam, Z. H. Mahmood, and N. Ara Sultana, "Utilization of low cost metals as back contact with Perovskite Solar Cell," 2017. [Online]. Available: https://www.researchgate.net/publication/323735275

[115] Iglesias, M.; et al. Carbon electrodes and low-cost structures for perovskite solar cells. Electronics 2021, 10, 1145. Available at: https://www.mdpi.com/2079-9292/10/10/1145

[116] Habesrotinger, S.N.; Ligtens, T.; Eberon, J.E.; Strunks, S.D.; Nicholas, R.J.; Snaith, H.J. Carbon electrodes for high-efficiency perovskite photovoltaic cells. Nano Letters 2014, 14, 5561-5568.

[117] Chang, H.; et al. Integration of carbon electrodes and contact architecture for perovskite solar cells. Advances in Photovoltaics: Research and Applications 2024. DOI: 10.1002/pip.70053.

[118] Chen, P., et al. Stabilization of perovskite solar cells through interfacial and electrode engineering. Communications Materials 2022. Available at: https://www.nature.com/articles/s43246-022-00281-z

[119] Khan, M. A., et al. Effect of hole-transporting material on perovskite solar cells with different metallic electrodes: SCAPS-1D simulation view. Scientific Reports 2023. Available at: https://pmc.ncbi.nlm.nih.gov/articles/PMC10258428/

[120] Michaelson, H. B. Occupational Function and Periodicity of Elements. Journal of Applied Physics 1977, 48, 4729–4733.

[121] Busch, K. A.; et al. Thermal and environmental stability of perovskite solar cells through contact and interface control. ACS Energy Letters 2016, 1, 428–435.

[122] Cha, J. H.; et al. Air-stable transparent heterojunction of silver iodide and copper iodide. ACS Materials and Interface Applications 2017. DOI: 10.1021/acsami.7b14378

[123] Ki, W.; Stombos, S. S.; Kanatzidis, M. J. "Lead-free perovskites": Current status and future prospects for tin-based perovskite solar cells. Advanced Materials 2019, 31, 1803230. DOI: 10.1002/adma.201803230.

[124] Slavny, A.H.; Ho, T.; Lindenburg, A.M.; Caronadasa, H.E. Long-life, charge-carrier bismuth halide perovskite for photovoltaic applications. Journal of the American Chemical Society 2016, 138, 2138-2141. DOI: 10.1021/jacs.5b13294.

[125] Maclure, E.T.; Paul, M.R.; Wendell, W.; Ertkin, E.C. AgBiX6 (X = Br, Cl): Novel lead-free, visible-light-absorbing halide perovskite semiconductor. Chemistry of Materials 2016, 28, 1348-1354.

[126] Huang, Y.-T.; Kavanagh, S.R.; Scanlon, D.O.; Walsh, A.; Hui, R.L.Z. Perovskite-inspired materials for photovoltaics and beyond—from design to devices. Nanotechnology 2021, 32, 132004. DOI: 10.1088/1361-6528/abcf6d.

[127] Hui, R.L.Z.; et al. Advances in lead-free, perovskite-inspired absorber materials for photovoltaics: charge transfer, defects, and device limitations. Advanced Functional Materials 2021, 2105898. DOI: 10.1002/adfm.202105898.

[128] Y. Raoui, H. Ez-Zahraouy, N. Tahiri, O. El Bounagui, S. Ahmad, and S. Kazim, "Performance analysis of MAPbI3 based perovskite solar cells employing diverse charge selective contacts: Simulation study," *Solar Energy*, vol. 193, pp. 948–955, Nov. 2019, doi: 10.1016/j.solener.2019.10.009.

[129] A. K. Kang, M. H. Zandi, and N. E. Gorji, "Simulation analysis of graphene contacted perovskite solar cells using SCAPS-1D," *Opt Quantum Electron*, vol. 51, no. 4, Apr. 2019, doi: 10.1007/s11082- 019-1802-3.

[130] S. Wang, T. Sakurai, W. Wen, and Y. Qi, "Energy Level Alignment at Interfaces in Metal Halide Perovskite Solar Cells," Nov. 23, 2018, *Wiley-VCH Verlag*. doi: 10.1002/admi.201800260.

[131] Muhammad Haneef, Sofia Tahir, Haitham A. Mahmoud, Adnan Ali, Arslan Ashfaq; Optimizing Lead-free MASnBr3 Perovskite Solar Cells for High-Efficiency and Long-Term Stability Using Graphene and Advanced Interface Layers. ACS Omega 13 February 2024; 9(6): 7053–7060. https://doi.org/10.1021/acsomega.3c08981.

[132] Sabbah, H.; Arayro, J.; Mezher, R. Numerical Simulation and Optimization of Highly Stable and Efficient Lead-Free Perovskite FA1−xCsxSnI3-Based Solar Cells Using SCAPS. Materials 2022, 15, 4761. https://doi.org/10.3390/ma15144761.

[133] Cheng-Min Tsai,1 Yu-Pei Lin,1 Murali Krishna Pola,1 Sudhakar Narra,1 Efat Jokar,1Yaw-Wen Yang2 and Eric Wei-Guang Diau, Control of Crystal Structures and Optical Properties with Hybrid Formamidinium and 2-Hydroxyethylammonium Cations for Mesoscopic Carbon-electrode Tin-based Perovskite Solar Cells, Downloaded from pubs.acs.org/aelccp/article-supplement/682482/pdf/nz8b01046_si_001/ by guest on 24 August 2026.

[134] Bidikoudi, M.; Simal, C.;Stathatos, E. Low-Toxicity Perovskite, Applications in Carbon Electrode, Perovskite Solar Cells—A Review. Electronics 2021, 10, 1145. https://doi.org/10.3390/electronics10101145.

[135] Mozhdeh Forouzandeh, Maryam Heidariramsheh, Hamid Reza Heydarnezhad, Hafez Nikbakht ,Maurizio Stefanelli, Luigi Vesce, Nima Taghavinia, Enhanced carbon-based back contact electrodes for perovskite solar cells: Effect of carbon paste composition on performance and stability, 10.1016/j.carbon.2024.119450.

[136] Yu Zhang; Bin Zhao; Lang Liu; Ning Wang, Interfacial Molecular Lock Enables Highly Efficient Tin Perovskite Solar Cells Interfacial Molecular Lock Enables Highly Efficient Tin Perovskite Solar Cells, ACS Appl. Mater. Interfaces (2023) 15 (46): 53362–53370. https://doi.org/10.1021/acsami.3c10146.

[137] Meng Li, Wei-Wei Zuo, Qiong Wang, Kai-Li Wang, Ming-Peng Zhuo, Hans Köbler,Christian E. Halbig, Siegfried Eigler,* Ying-Guo Yang, Xing-Yu Gao, Zhao-Kui Wang,*Yongfang Li, and Antonio Abat, Ultrathin Nanosheets of Oxo-functionalized GrapheneInhibit the Ion Migration in Perovskite Solar Cells, DOI: 10.1002/aenm.201902653.

[138] P. Wang, N. Li, L. Yang, C. Dal Anesi, A. K. Jena, S.-I. Sasaki, T. Miyasaka, H. Tamiaki, "Chlorophyll-Derivative-Sensitized Titanium Dioxide (TiO_2) Electron-Transport Layer for Record-Efficiency Double-Perovskite ($Cs_2AgBiBr_6$) Solar Cells," Journal of the American Chemical Society (JACS), Vol. 143, No. 5, pp. 2207–2212, PubMed ID (PMID): 33522803, 2021.

(This work is licensed under a Creative Commons Attribution 4.0 International License.)

International Journal of Engineering Research & Technology (IJERT)
ISSN: 2278-0181
Vol. 15 Issue 11 , November - 2026

[139] Wafa' Ayaydah, Eman Raddad, Zafer Hawash, Sn-Based Perovskite Solar Cells towards High Stability and Performance, Micromachines (MDPI), 2023, Vol. 14, Issue 4, Article 806, PMC10143209

(This work is licensed under a Creative Commons Attribution 4.0 International License.)